Annu. Rev. Biophys. Biomol. Struct. 1997. 26:181–222

BIOMOLECULAR DYNAMICS AT LONG TIMESTEPS: Bridging the Timescale Gap Between Simulation and Experimentation

Tamar Schlick, Eric Barth, and Margaret Mandziuk
The Howard Hughes Medical Institute and New York University, Department of Chemistry and Courant Institute of Mathematical Sciences, 251 Mercer Street, New York, NY 10012

KEY WORDS: molecular and Langevin dynamics, numerical integration, linearized models, normal modes, multiple timesteps

ABSTRACT

Innovative algorithms have been developed during the past decade for simulating Newtonian physics for macromolecules. A major goal is alleviation of the severe requirement that the integration timestep be small enough to resolve the fastest components of the motion and thus guarantee numerical stability. This timestep problem is challenging if strictly faster methods with the same all-atom resolution at small timesteps are sought. Mathematical techniques that have worked well in other multiple-timescale contexts—where the fast motions are rapidly decaying or largely decoupled from others—have not been as successful for biomolecules, where vibrational coupling is strong.

This review examines general issues that limit the timestep and describes available methods (constrained, reduced-variable, implicit, symplectic, multiple-timestep, and normal-mode-based schemes). A section compares results of selected integrators for a model dipeptide, assessing physical and numerical performance. Included is our dual timestep method LN, which relies on an approximate linearization of the equations of motion every Δt interval (5 fs or less), the solution of which is obtained by explicit integration at the inner timestep $\Delta\tau$ (e.g., 0.5 fs). LN is computationally competitive, providing 4–5 speedup factors, and results are in good agreement, in comparison to 0.5 fs trajectories.

These collective algorithmic efforts help fill the gap between the time range that can be simulated and the timespans of major biological interest (milliseconds and longer). Still, only a hierarchy of models and methods, along with

1056-8700/97/0610-0181$08.00

experimentational improvements, will ultimately give theoretical modeling the status of partner with experiment.

CONTENTS

INTRODUCTION

The Time Race

In the world of computation, time is the enemy. Scientists wage a battle of wits to squeeze as many computations as they can into the shortest possible span of time. The larger and more complex the problem, the more cunning their techniques must be (82).

The above battle refers to forecasting the weather, where the development of rapidly converging and computationally tractable large-scale optimization techniques is key. Yet, the statement rings at least equally true for simulating biomolecular motion on modern computers (89), where the crucial numerical techniques for integrating the equations of motion have ranged from brute-force to ingenious. In molecular dynamics (MD) simulations, insights into molecular flexibility and activity are sought by numerically following molecular configurations in time according to Newtonian physics (3, 21, 64). In theory, MD simulations can bridge spatial and temporal resolution and thus capture molecular motion over a wide range of thermally accessible states. In practice, the numerical timestep problem has limited most applications to straightforward

Table 1 Some typical vibrational modes[a]

Vibrational mode	Wavelength of absorption [cm^{-1}] ($1/\lambda$)	Absorption frequency [s^{-1}] ($\nu = c/\lambda$)	Period [fs] ($1/\nu$)	Period/π [fs]
O−H stretch N−H stretch	3200–3600	1.0×10^{14}	9.8	3.1
C−H stretch	3000	9.0×10^{13}	11.1	3.5
O−C−O asymmetric stretch	2400	7.2×10^{13}	13.9	4.5
C≡C, C≡N stretch	2100	6.3×10^{13}	15.9	5.1
C=O (carbonyl) stretch C=C stretch	1700	5.1×10^{13}	19.6	6.2
H−O−H bend	1600	4.8×10^{13}	20.8	6.4
C−N−H bend H−N−H bend C=C (aromatic) stretch	1500	4.5×10^{13}	22.2	7.1
C−N stretch (amines)	1250	3.8×10^{13}	26.2	8.4
Water Libration (rocking)	800	2.4×10^{13}	41.7	13
O−C−O bending C=C−H bending (alkenes) C=C−H bending (aromatic)	700	2.1×10^{13}	47.6	15

[a]All values are approximate; a range is associated with each motion depending on the system. The value of $c = 3.00 \times 10^{10}$ cm s^{-1}. The last column indicates the timestep limit for leap-frog stability for a harmonic oscillator: $\Delta t < 2/\omega = 2/(2\pi\nu)$.

integration with very small timesteps compared to the motion of major interest. Consequently, the total length of current trajectories at atomic resolution is limited to the nanosecond timescale.

Our battle in the world of biomolecular dynamics is to reliably simulate as large a timespan as possible in the smallest amount of computational time. The reliability issue is a separate topic in its own right, since our force fields are approximate, quantum effects are ignored, and many other model assumptions or special simulation protocols are applied. In addition to these approximations, single-trajectory results must be assessed in the framework of statistical mechanics. Simulations are computationally taxing because of the typical expense of computing the Newtonian forces for a system of thousands of atoms—the solute and solvent—at each 1-fs timestep. Since conformational changes in macromolecules occur on a continuum of timescales ranging from 10^{-12} to 10^{2} s (see Table 1 for the high-frequency end), considerable research has focused on (*a*) developing algorithms that alleviate the severe stability requirement dictated by the high-frequency vibrational modes, and (*b*) exploiting high-speed parallel computer technology to accelerate MD simulations (16).

Strong Vibrational Coupling in Biomolecules

A significant finding that emerged from these algorithmic efforts for increasing the timestep in biomolecular simulations (36, 41, 69, 89, 97, 102, 116) is the unexpected difficulty of this challenge if one strictly seeks faster methods with the same all-atom resolution of small-timestep trajectories. Vibrational modes are intricately coupled in biomolecules such as proteins and nucleic acids. Therefore, mathematical techniques that have worked well in other multiple-timescale contexts where the fast motions are decaying rapidly rather than oscillatory (e.g. in chemical reactions with known reactants and products), or are largely decoupled from the others (e.g. in fullerenes), have not been directly applicable, or as effective, for biomolecules. For example, standard high-stability implicit schemes for stiff differential equations, such as implicit-Euler (IE) (43, 73, 95) and implicit-midpoint (IM) (57), are unsatisfactory for proteins and nucleic acids at atomic resolution at large timesteps because of numerical damping (69, 96, 119) and resonance (57) problems, respectively. Implicit methods are also computationally expensive since solution of a nonlinear system is required at each timestep (48, 49, 120, 121). Algorithms based on substructuring (110) require substantial tailoring and perhaps relaxation of goals (i.e. approximate rather than accurate reproduction of small-timestep trajectories) for biomolecular applications, and multiple-timestep (MTS) methods that achieve a factor of 20 or more speed-up for fullerenes (74) yield much more modest factors (e.g. 4) for macromolecules (45, 116).

The intricate vibrational coupling of the multiscale modes associated with globular systems necessitates good resolution of the high end of the spectrum in order to capture the slower, large-scale motions. Constraining the fast modes is effective when bond-length stretching is suppressed but not when the bond-angle flexibility is also eliminated (111). For good resolution of the high-frequency motion, MTS methods often use a very small timestep (0.25 fs) for the highest-frequency class (122).

Figure 1 illustrates this point. The figure displays the frequency spectrum for a blocked alanine residue (N-Acetylalanyl N′-Methylamide, 22 atoms), known commonly as an "alanine dipeptide", as obtained from MD simulations using various protocols. These power spectra were obtained from velocity time series (14), with the Fast Fourier Transform routine (Sande-Tukey FFT) (59). All MD simulations were performed in the CHARMM program (19) using the Verlet integrator (113) at a timestep of 1 fs over 2^{14} steps ($\sim$17 ps), but different constraint procedures were enforced via SHAKE (87) in some cases, as follows: (*a*) no constraints, (*b*) constraints on bonds involving hydrogens only, (*c*) constraints on all bonds, and (*d*) constraints on all bonds and bond angles involving hydrogens. In parts *b* and *c*, bonds were constrained to their equilibrium values. In part *d*, constraints were made to the starting values

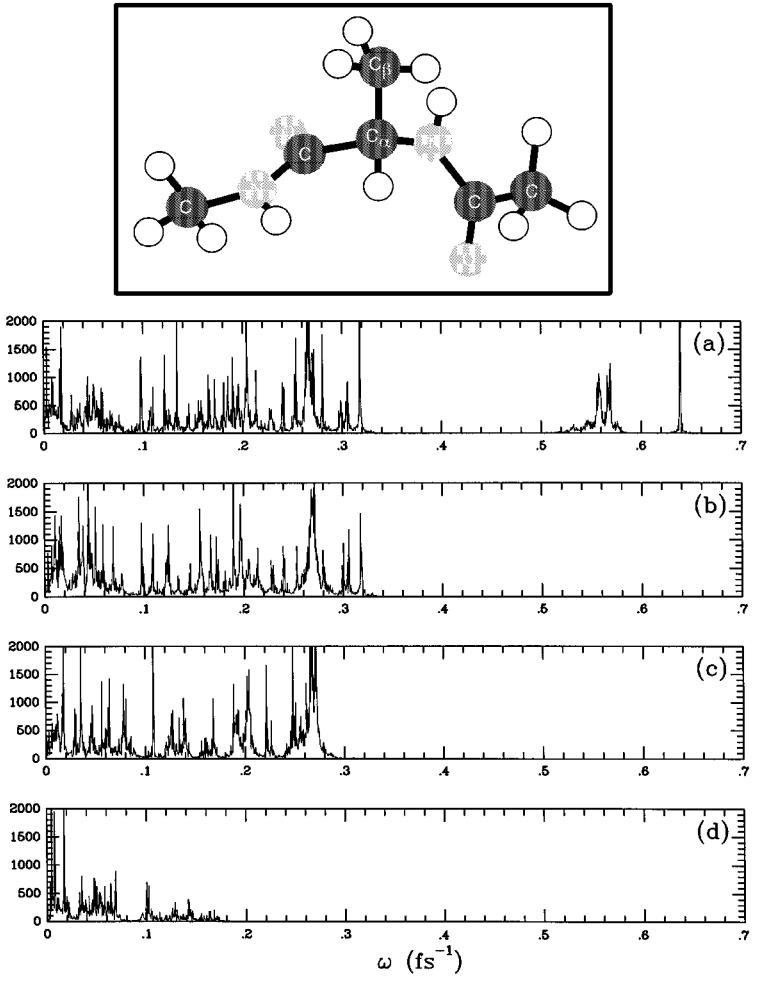

Figure 1 The frequency spectrum for a model of alanine dipeptide (*top*), as obtained from 17-ps MD simulations with CHARMM (19) using various constraint protocols via SHAKE (87) with an improved protocol (12), in association with Verlet integration at $\Delta t = 1$ fs: (*a*) no constraints; (*b*) constraints only on bonds involving hydrogens; (*c*) constraints on all bonds; and (*d*) constraints on all bonds and on bond angles involving hydrogens. The frequency spectra were obtained from velocity time series (14), with the Fast Fourier Transform routine (Sande-Tukey FFT) (59). The spectral heights are relative.

associated with the minimized conformation, and the implementation of bond-angle constraints was performed with an improved algorithm (12).

The two highest-frequency ranges observed in the unconstrained trajectory (Figure 1*a*) can be associated with bond stretches for N–H (period $P = 2\pi/\omega \approx 10$ fs) and C–H (P $\approx$ 11 fs). When the bonds involving hydrogens are constrained, these two regions of the spectrum are eliminated and a shift to the beginning range of the angle-bending modes and the lower-frequency bond stretches results (Figure 1*b*). The highest frequency now resolved corresponds to about 20 fs. When all bonds are constrained (Figure 1*c*), only a slight shift can be noted in the spectrum, and the fastest period corresponds to 23 fs. This effect illustrates the very short gap in the vibrational spectrum between the heavy-atom bond-stretching and light-atom angle-bending modes in biomolecules (see also Table 1). When the angles involving hydrogens are also constrained (Figure 1*d*), the frequency spectrum shifts further, and the highest frequency has a period of 35 fs; in addition, a marked lowering of the amplitudes of the resolved frequencies is evident in comparison to parts *a–c* of Figure 1. This effect points to the strong vibrational coupling in biomolecules and the severity of both the numerical integration problem and the difficulty of obtaining physically meaningful results without resolving the high-frequency modes.

Simulation Classes

Many significant biological problems involving macromolecules can be tackled on various levels and with algorithms that range from purely stochastic (i.e. by generating disconnected configurational ensembles) to those that guarantee continuous dynamics (i.e. by solving deterministic equations). It is essential that the simulation goal be tightly coupled to the problem at hand. Consequently, it is inappropriate (96) to apply methods intended for biomolecules to special systems such as fluids, and/or to subject these methods to irrelevant questions (118).

Configurational propagators for biomolecules can be divided into three broad classes: (*a*) continuous and accurate dynamics, (*b*) continuous but approximate dynamics, and (*c*) sampling. The first group includes schemes for capturing continuous motion that reproduce the dynamic trajectory as obtained with a small-timestep method. This small timestep must adequately resolve the highest frequency of the system (e.g. $1/20$ the size of the fastest period). For biomolecules this means $\Delta t \approx 0.5$ fs corresponding to the 10-fs period of an O–H or N–H stretch (see Table 1). From simulations in this first class, reaction pathways can be deduced and transition rates estimated, though a rigorous global analysis is also required (i.e. ensemble properties in the framework of statistical mechanics) (67). Dynamic simulations can also be used for statistical averaging in phase space, though special care must be exercised for the highly correlated data.

The second group of methods relaxes the accurate reproduction of short-time processes but seeks to capture essential features of the system over longer times.

The many schemes in this class range from Brownian dynamics, for example, where inertial effects are small (39, 46a), to pseudodynamic methods (28, 44, 106), which might combine elements of minimization and dynamics. Information extracted from these trajectories involves, for instance, translational and rotational diffusion constants (46a), the structure of a folded protein (1), or insights into folding pathways (28, 44).

The third class includes techniques for efficient sampling of the large configuration space accessible to biomolecules in solution (18, 30, 34). Here, ensemble properties can suggest average behavior as a function of key parameters (e.g. the salt concentration effects on supercoiled DNA; 114) and provide average energetic and structural properties for analysis. Techniques in this class might also be used to find the global minimum of a given biomolecule or to refine experimental data (23).

Overview

This review focuses on the computational, physical, and modeling issues involved in designing innovative integrators or configurational propagators for biomolecules. We describe algorithms based on continuous dynamics and point to promising directions that will help bridge the gap between the timescales accessed by computer and those resolved by experimentation. Readers may wish to refer to three recent reviews on the topic (31, 53, 65).

The next section examines some general issues that limit the timestep in MD simulations of biomolecules. Various methods in the continuous and accurate dynamics class that are, or have potential to be, competitive schemes are then presented.[1] These include constrained and torsion (i.e. reduced-variable simulations) dynamics, implicit and symplectic schemes, and multiple-timestep and normal-mode-based methods. The last class includes our LN algorithm, so named for its origin in a Langevin/normal modes scheme. This dual timestep method ($\Delta\tau$, Δt) is based on a simple idea: explicit subintegration—using an inner timestep $\Delta\tau$ (e.g. 0.5 fs)—of a cheaply constructed linearized model for the equations of motion—formulated every Δt interval (5 fs or less). Since the subintegration process does not require new force evaluations, as does every step of standard MD integration, LN can be computationally competitive (13). Furthermore, since the harmonic approximation is reasonable over the short interval Δt, results are in good agreement with small-timestep simulations. We also include in this review comparative numerical experiments involving the various methods presented to highlight the physical and computational facets discussed throughout. We conclude with a perspective regarding the future of MD algorithms.

[1]Development of novel approaches that might initially appear impractical for macromolecules can lead to unexpected surprises, and their development should not be curtailed on the basis of computational performance alone (13).

THE TIMESTEP PROBLEM

Numerical integrators require the timestep to be small enough with respect to the most rapid component of the motion to guarantee stable numerical behavior (42, 43, 89). This is especially important for the relatively low-order explicit methods used in biomolecular MD.[2] In MD, we solve the initial-value ordinary differential equation $y' = f(y)$, where y is the collective vector of positions and velocity ($\{X, V\}$) and f is a nonlinear function representing the configuration-dependent force vector. We can express this relation by the following system of two first-order differential equations:

$$\mathbf{M}\dot{V}(t) = -\nabla E(X(t)), \tag{1a}$$

$$\dot{X}(t) = V(t), \tag{1b}$$

where $\mathbf{M}$ is the diagonal mass matrix, $\nabla E(X(t))$ is the gradient vector of the potential energy E, and the dot superscripts denote differentiation with respect to time t. Additional terms can be added to the right side of Equation 1a, such as in the Langevin framework (described below).

Explicit and Implicit Schemes

In explicit schemes, solutions are simple to propagate since they take the symbolic form $y^{n+1} = g(y^n, \Delta t, \ldots)$, where g is some nonlinear function and y^n is the difference-equation approximation to the solution y at time $n\Delta t$. Thus, the calculation of y^{n+1} depends on previously known quantities ($y^n, y^{n-1}, \ldots$). Implicit integrators, in contrast, define the final solution as a function of both initial and final variables: $y^{n+1} = h(y^{n+1}, y^n, \Delta t, \ldots)$ and thus generally require solution of a coupled nonlinear equation at each timestep. This incorporation of future information helps avoid stability problems associated with purely extrapolative techniques (35).

For example, the well known (explicit) leap-frog method applied to System 1 propagates positions and velocity on the basis of the following difference equations (3):

$$\mathbf{M}(V^{n+\frac{1}{2}} - V^{n-\frac{1}{2}})/\Delta t = -\nabla E(X^n), \tag{2a}$$

$$(X^{n+1} - X^n)/\Delta t = V^{n+\frac{1}{2}}. \tag{2b}$$

This formulation is equivalent to Verlet's scheme (113), but it avoids the instability arising from rounding errors present in the latter. The leap-frog method can be started by using the relation $V^{1/2} = V^0 - (\Delta t/2)\nabla E(X^0)$. Whole-step velocities can be obtained by averaging $V^n = (V^{n+1/2} + V^{n-1/2})/2$.

[2] Although higher-order methods have been attempted, low-order (e.g. 2) integrators are adequate for MD given the inaccuracy in the governing force functions, combined with the goal of simulating motion reasonably and efficiently over as large a time interval as possible.

The implicit-midpoint scheme relies on the discretization

$$\mathbf{M}(V^{n+1} - V^n)/\Delta t = -\nabla E\left[\frac{1}{2}(X^n + X^{n+1})\right], \tag{3a}$$

$$(X^{n+1} - X^n)/\Delta t = (V^n + V^{n+1})/2. \tag{3b}$$

This nonlinear system can be solved by obtaining X^{n+1} as a minimum (73) of

$$\Phi(X) = \frac{1}{2}\left(X - X_0^n\right)^T \mathbf{M}\left(X - X_0^n\right) + (\Delta t)^2 E\left(\frac{X + X^n}{2}\right), \tag{3c}$$

$$X_0^n = X^n + \Delta t\, V^n \tag{3d}$$

(where the superscript T denotes a vector transpose), and then solving for V^{n+1} via Equation 3b).

The general condition limiting the timestep size for numerical stability is derived on the basis of a linear reference system. For example, a restriction $\Delta t < 2/\omega = P/\pi$ applies to the LF method for a harmonic oscillator of natural frequency ω and period P (121). Such a condition, however, serves as a loose upper bound for MD simulations, where the forces are highly nonlinear. Introduced stochasticity, as in the form of the Langevin equation, further restricts the timestep: $\Delta t < (2\omega - \gamma)/\omega^2 = P/\pi - (P^2\gamma)/4\pi^2$, where γ is the damping constant (121). Indeed, with the second-order Verlet method for MD, a timestep much smaller than 3.2 fs, and much less than 7 fs when all bonds are constrained (see Table 1 and Figure 1*c*), must be used to provide good behavior in practice. Although implicit schemes are unconditionally stable according to linear analysis (26), nonlinear effects introduce instability (57a).

Culprits of the Timestep Limitation and Instability

The severe timestep limitation observed for biomolecular dynamics stems from a combination of at least the following three culprits: (*a*) classic numerical instability, (*b*) resonance, and (*c*) van der Waals collisions. In addition, systematic and random errors introduce inaccuracies and instability into MD simulations.

The first and most common factor—numerical instability resulting from the timestep size—can be verified by an error pattern that grows steadily and systematically with the timestep until a threshold is reached (e.g. 89). At that point, quantities grow uncontrollably from step to step and quickly exceed the computer's finite-size capabilities in the course of the simulation. Errors of this type are scheme and model dependent, aggravated by nonlinearity (121), and show instability at smaller timesteps for higher-order methods.

In contrast, resonance is an integrator-induced corruption of a system's dynamics (51, 66, 98, 57a). Essentially, resonance occurs at special timesteps that are related in a complex way to the various timescales of the motion (57). At those timesteps, a concerted effect stemming from one component of the motion

(e.g. heating of a bond-stretch vibrational mode) leads to very large energetic fluctuations or instability (e.g. bond rupture). Thus, resonance problems lead to erratic, rather than systematic, error patterns as a function of timestep. They are also method and system dependent (99), occur for both implicit and explicit schemes [e.g. Verlet and IM (57)], and depend strongly on the fastest frequency in the system and possibly on the coupling strength to other vibrational modes.

Figure 2 shows an example of bond breaking, as obtained by IM integration of a deoxycytidine model (90) with a quartic bond potential. (A similar pattern was also found for a harmonic potential; M Mandziuk & T Schlick, unpublished data). Resonance has been demonstrated for symplectic integrators, such as Verlet and IM, which are typically associated with favorable properties; however, methods that are nondamping for linear problems, (e.g. symplectic), can also have instabilities resulting from nonlinear resonances (57a).

The third possible culprit stems from nonbonded interactions. Van der Waals collisions may cause numerical problems for macromolecules because of the stiff and highly nonlinear distance-dependence of the governing potential (r^{-12}, where r is an interatomic distance; see Figure 3 for examples of local harmonic approximations to the Lennard-Jones potential). Unless the timestep is quite small, atoms in globular systems come into intimate contact, thereby raising the nonbonded energy sharply. This leads to structural distortion and sudden, localized addition of kinetic energy. This behavior can be particularly aggravated by resonance tendencies. These tendencies provide large energies to selected vibrational modes (i.e. a bond stretch), which in turn can be transferred to other modes. Such collisional problems should be highly system dependent (i.e. affected by molecular size and solvent modeling) and may be less dependent on the scheme.

Some suggestions of timestep limitations due to nonlinear interactions come from demonstrations that smaller timesteps must be used for larger molecular systems. For example, Gibson & Scheraga found, by application of their torsion-angle dynamics method with a variable timestep to two blocked amino acid residues, that timesteps around 30 fs worked well for a smaller model in contrast to values $\leq$20 fs needed for a larger model peptide (36). Watanabe & Karplus found the same trend in their MTS applications (116). Results with our integration approach, based on force linearization and implicit discretization (termed LIN for Langevin/implicit integration/normal modes) (119, 120), showed that timesteps of 30 fs were satisfactory for a model dipeptide but were far too large for the small protein BPTI (bovine pancreatic trypsin inhibitor), where Δt had to be reduced by half (13). Extreme trajectory sensitivity to the Lennard-Jones parameters (27) also points to the important role of collisions on MD integration.

Systematic errors enter biomolecular simulations from various sources, such as truncated multipole expansions, truncation and/or smoothing procedures

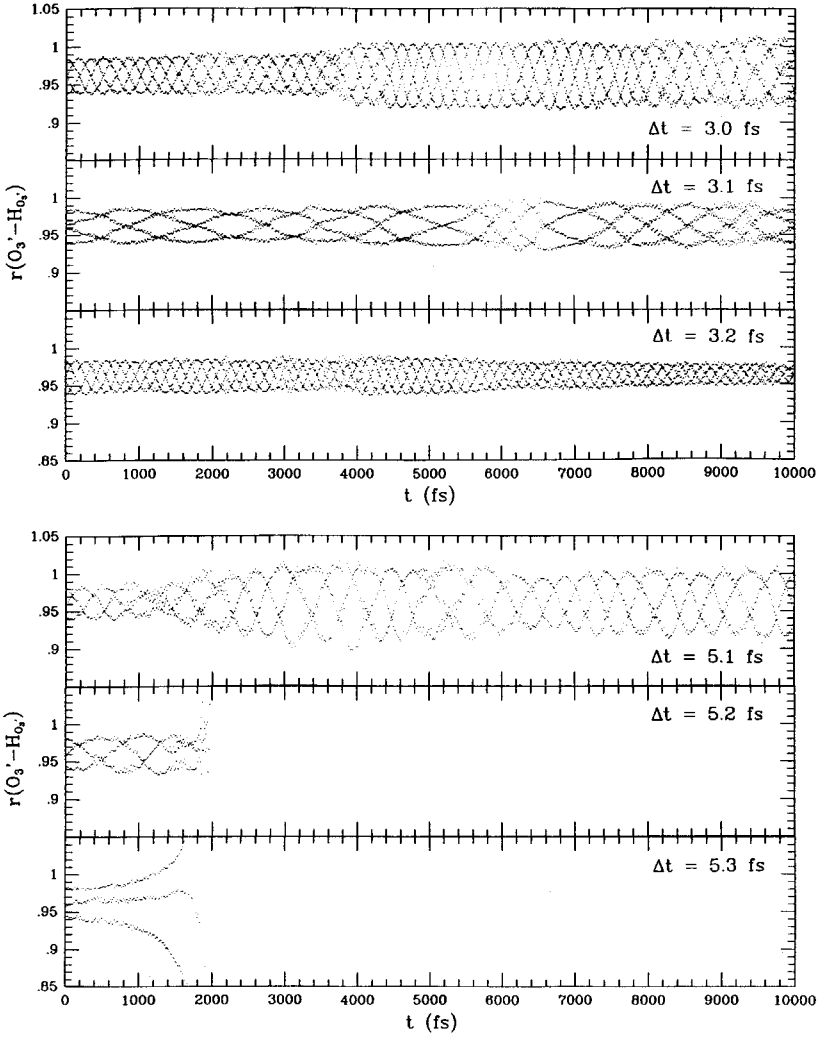

Figure 2 Third and fourth order resonances for a deoxycytidine system integrated by the implicit-midpoint scheme at various timesteps. Shown is the length of an O–H bond in a model deoxycytidine system (90) as obtained in simulations at various timestep values. The bond-length potential is quartic, with force constants adapted from the AMBER potential, making resonance tendencies much more pronounced in relation to the standard harmonic potential.

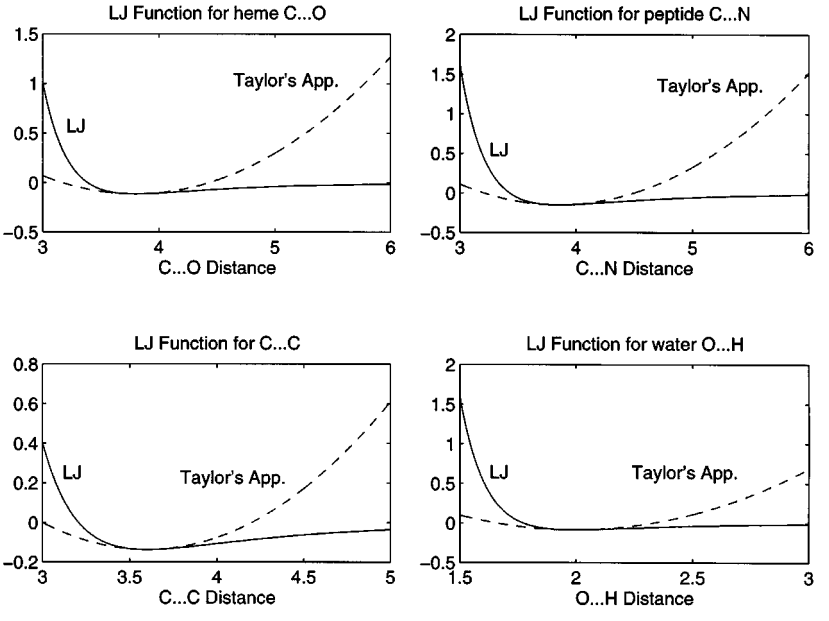

Figure 3 Harmonic approximations to various Lennard-Jones functions.

(101), and computer roundoff (finite precision arithmetic). Random or spurious errors, including inconsistency problems, can creep in from a variety of sources, such as the simulation protocol (e.g. equilibration procedure, starting structure, minimizer, treatment of energy fluctuations), the finite length of the trajectory (e.g. finite ensemble averages), finite length of the pseudorandom number generator, or program errors.

Systematic and random errors are both common and specific to the various molecular mechanics and dynamics programs available today. They also depend on the computer precision, architecture, and compiler. Although such problems are well known to practitioners, little has been written about them. Recent exceptions include Elofsson & Nilsson (32) who investigated the consistency of MD simulations by comparing 30 protein simulations differing in solvent representation and protocols; they found great sensitivity of overall fluctuations to the starting structure and suggested that several shorter simulations span conformation space better than one long one. Auffinger et al (8) demonstrated the divergence of ten 100-ps trajectories of tRNA in solvent and salt—from the initial X-ray structure as well as from one another—when initial conditions and parameters were varied. Consistency problems also emerged: For example, the divergence was faster when the equilibration time was extended.

This divergence was later attributed to a short (8 Å) cutoff radius for the long-range solvent interactions, since doubling the value improved the consistency between two MD trajectories (9). Van Gunsteren and coworkers (46) showed that, depending on the computational procedure used to induce an unfolding process for lysozyme, different qualitative behavior could be observed. More recently, Daura et al (27) demonstrated the sensitivity of solvated protein dynamics to the van der Waals parameters describing water-protein and protein-protein interactions. This sensitivity further points to the role of the van der Waals interactions in limiting the timestep, as suggested above. These reports also illustrate the need for an error or assessment framework for MD simulations. Such a framework has been described in the linear case, for explicit (72) and implicit (67) integration, but extensions to the nonlinear case are difficult.

LARGE-TIMESTEP TECHNIQUES FOR CONTINUOUS DYNAMICS

Constrained Dynamics

In overcoming the timestep problem in MD simulations, any successful algorithm must decrease the ratio of force calculations per time unit from the Verlet standard of about two per femtosecond. One possibility is to replace the highest-frequency interactions, typically modeled in biomolecular potentials by:

$$E_{\text{bond}} = \frac{\kappa}{2}(r_{ij} - \overline{r_{ij}})^2,$$

where r_{ij} is an interatomic distance of equilibrium value $\overline{r_{ij}}$ and κ is a force constant, by algebraic constraints:

$$g_i = r_{jk}^2 - \overline{r_{jk}}^2 = 0.$$

Using the formalism of Lagrange multipliers, we have:

$$\begin{aligned} \mathbf{M}\dot{V}(t) &= -\nabla E(X(t)) - g'(X(t))^T \lambda, \\ \dot{X}(t) &= V(t), \\ g(X(t)) &= 0, \end{aligned} \tag{4}$$

where $g(X(t))$ is a vector with entries g_i containing the individual constraints, and the vector of Lagrange multipliers, λ, is proportional to the constraint force.

In 1977, Ryckaert et al (87) introduced the SHAKE method, based on the leap-frog/Verlet scheme of System 2, for discretization of the constrained

equations:

$$\begin{aligned}(V^{n+\frac{1}{2}} - V^{n-\frac{1}{2}})/\Delta t &= -\nabla E(X^n) - g'(X^n)^T \lambda^n, \\ (X^{n+1} - X^n)/(\Delta t) &= V^{n+\frac{1}{2}}, \\ g(X^{n+1}) &= 0.\end{aligned} \tag{5}$$

Like the Verlet method, the forces $-\nabla E$ must be computed only once per step. However, the m constraints also require, at each timestep, the solution of a nonlinear system of m equations in the m unknowns $\{\lambda_i\}$. Thus, the SHAKE method is semi-explicit. RATTLE is a self-starting version of SHAKE (6). Similar techniques have been proposed for constraining other internal degrees of freedom (104), and direct methods have been developed for the special case of rigid water molecules (68). Recently, Leimkuhler & Skeel (52) showed that the RATTLE method is symplectic and that SHAKE, while not symplectic, yields identical positions and only slightly perturbed velocities.

With the fastest vibrations removed from the model, the integration timestep can be lengthened, resulting in a typical force calculation per time ratio of 0.5 per femtosecond. This computational advantage must be balanced against the additional work required to solve the nonlinear equations of constraints. Each proposed constrained model is thus accompanied by a practical numerical algorithm. For the time discretization of Equation 5, an iterative scheme for solving the nonlinear equations was presented (87), where the individual constraints are imposed sequentially to reset the coordinates that result from an unconstrained Verlet step. This iterative scheme is used widely because it is simple and requires modest computer memory. However, the SHAKE iteration can converge very slowly, or even fail to converge, for complex bond geometries (12). Barth et al (12) proposed enhancements that do not suffer significant performance degradation in the presence of highly coupled bond structures and that can reduce the computational cost by 50% for typical cases. They reported that the improved solution process of the constraint equations requires only about 10% of the total computation time, a modest price to pay for the twofold decrease in the force-evaluation-per-time ratio.

The computational advantage of constrained models is clear, but the agreement between the constrained and unconstrained trajectories depends on the formulation details of the constrained scheme. As mentioned above, van Gunsteren & Karplus (112) showed through simulations of the protein BPTI in a vacuum that the use of fixed bond lengths does not significantly alter the dynamical properties of the system, whereas fixing bond angles does. Similar conclusions for decane molecules were reported (105). Still, the former study reported suboptimal data for the angle constraints as a result of the slow (or lack of) convergence in the SHAKE iteration. The latter work encountered no such difficulty because a simpler carbon chain molecule was considered. In general,

angle constraints must be imposed with care to avoid overdetermination and singularities in the constraint equations. Our data for Figure 1 came from trajectories computed using SHAKE enhancements (12), implemented into CHARMM version 23f4. We found that the traditional SHAKE iteration required thousands of iterations when angles involving hydrogen atoms were constrained, unlike the approximate Newton methods, which showed no significant degradation in performance. In addition, constraining all bond angles can restrict torsion-angle motion, which in turn changes the overall dynamics. Such models are closely related to the reduced-variable and torsion-space formulations discussed below.

The power spectrum presented in Figure 1 suggests two effective constrained formulations among the three attempted: fixed light-atom bonds, or fixed bonds plus fixed light-atom angles. Results presented here suggest that the latter procedure might not provide an acceptable balance between efficiency and modeling accuracy. More sophisticated constrained dynamic formulations, which include corrections for coupling among modes, such as on the basis of the Fixman potential used in statistical mechanics, might be necessary, as was shown in for the torsion dynamics of a butane molecule (81). These results showed close agreement with unconstrained Langevin simulations; however, the increased complexity is substantial (78, 80). A different potential, the Rubin-Unger form (84), has also been suggested (17).

Torsion Dynamics

The number of independent variables can be reduced more naturally by modeling the system in generalized coordinates (86, 62, 2, 36, 56). Usually, bond lengths and bond angles are kept rigid, and dynamic simulations are performed in torsion space. The time evolution of the system is obtained by integrating Lagrange's equations of motion in generalized coordinates. Since the rigorous derivation of these equations is complex, approximations must be introduced in practice.

Ryckaert & Bellemans (86) used a generalized coordinate approach to study n-alkanes, in which only linear terms were retained, limiting the feasible timestep. Mazur and Abagyan (2, 62) extended this formulation to include nonlinear terms, using $\Delta t \approx 9$ fs in an all-atom representation of an alanine nonapeptide (63). Resorting to an extended-atom representation (i.e. removing methyl group rotations), and fixing the torsion angle of the hydroxyl group at the C-terminus, they increased the timestep to 13 fs, while keeping the energy fluctuations in the same range of unconstrained, all-atom trajectory at $\Delta t = 1$ fs (63). Although this timestep increase is significant, a matrix inversion is required at every timestep, limiting applications to large biomolecules. Implementation details can also be system dependent (63).

In Gibson & Scheraga's (36) variant of the generalized coordinate approach, Lagrange's equations are solved with a quadratic approximation to the

generalized force, and the variable timestep is determined on the basis of the relative magnitude of the neglected third derivative of the potential. This approach allows the timestep to be extended to 15–30 fs for small model systems.

Another formulation for torsion-angle dynamics is based on recursive algorithms for rigid body dynamics (10). Due to the nonseparability of the equations of motion, nonsymplectic integrators are used. The feasible timestep, however, is shorter than in the above approaches: 2 fs (83) and 2–4 fs (109). This observation may also be related to the higher temperature used in these simulations.

A major drawback of torsion dynamics is its distortion of the effective potential. Because barriers among configurational states are elevated, transitions are less probable. Therefore, torsion-angle dynamics schemes are probably most useful at higher temperatures, for sampling purposes.

Symplectic Schemes

Symplectic methods form a special class of numerical integrators for conservative systems that possess favorable theoretical and numerical properties (88). Development of symplectic integrators has involved significant interplay among mathematicians, physicists, and chemists. Seminal work (50) was done by physicists and mathematicians, both on explicit (85) and implicit (25) schemes, and these ideas have quickly filtered into the chemistry community (38).

In applications of symplectic schemes to classical Hamiltonian systems, the time evolution corresponds to a canonical transformation (37). This transformation implies strong conservation properties, such as preservation of areas in phase space (Liouville's operator). As a consequence of such conservation laws, symplectic schemes cannot conserve energy exactly, but they exhibit long-time stability (e.g. small energy fluctuations when the timestep is small) and often better performance than nonsymplectic methods of the same order of accuracy and timestep. Symplectic integrators often possess a time reversibility property.

The performance observed for the widely used Verlet integrator, for example, can be explained by its symplecticness (85). Other integrators for MD that seek reversibility and symplecticness include multiple-timestep (41, 108) and predictor-corrector (60) methods,[3] as well as techniques for extended systems generating canonical and isothermal-isobatic ensembles (61). The symplecticness of the impulse MTS method has been noted (15). These integrators may also be used for quantum dynamical applications, such as for solving the Schrödinger equation in the multichannel radial form (58).

Although symplecticness produces good results in the small-timestep regime, improved behavior in the larger-timestep range is not guaranteed. For example, the strong conservation property of integral invariants can lead to undesirable global coupling of energy components, such as opposing trends for the kinetic

[3]The predictor-corrector method (60) is symplectic, but only in phase space of double the dimension.

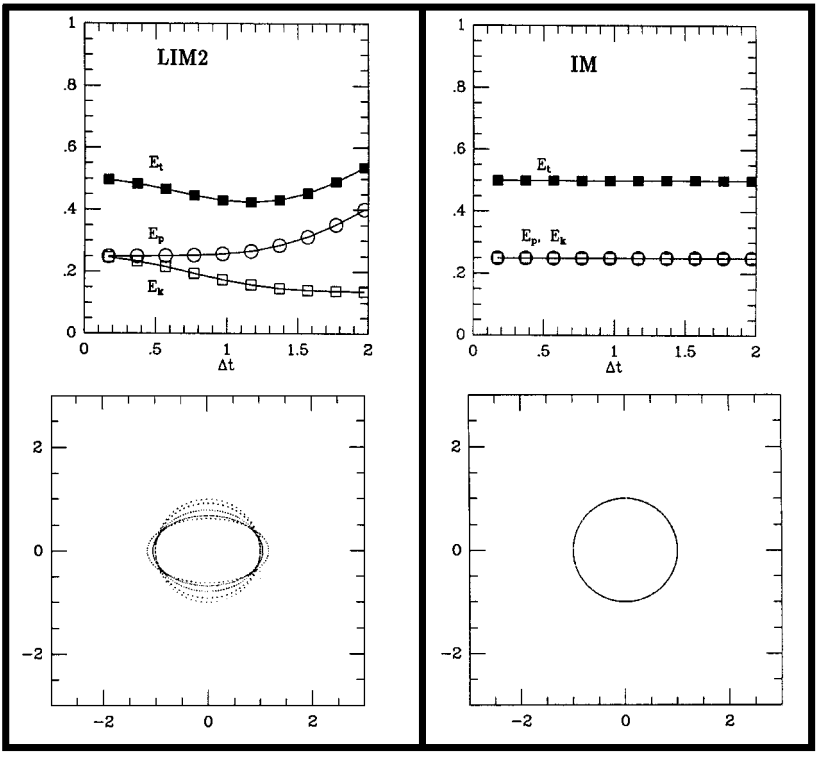

Figure 4 Harmonic oscillator average energy trends (*top*) and phase diagrams (*bottom*) as a function of timestep for two second-order, symplectic implicit integrators: LIM2 (121) (*left*) and IM (*right*) for Newtonian dynamics. The oscillator has unit mass, unit angular frequency ω, and initial total energy corresponding to 0.5 units. The governing propagation schemes are, for LIM2: $x^{n+1} - 2x^n + x^{n-1} = -\omega^2\ \Delta t^2(x^{n+1} + x^{n-1})/2$, and IM: $(v^{n+1} - v^n) = -\Delta t\ \omega^2(x^n + x^{n+1})/2$, with $(x^{n+1} - x^n) = \Delta t\,(v^n + v^{n+1})/2$. The smallest timestep, 0.2, is roughly 1/30 of a period, and the largest value is 1.95, about 1/3 the period. The symbols E_t, E_p, and E_k correspond to the total, potential, and kinetic energy components.

and potential energy components (67). This coupling has been observed for the implicit symplectic method LIM2 (121), but it may also be the result of an error constant five times greater than leap-frog/Verlet (57a). Shown in Figure 4 are average energy trends and phase diagrams as a function of timestep for a harmonic oscillator, as obtained by the two second-order implicit symplectic schemes LIM2 and IM for Newtonian dynamics. Figure 5 shows the analogous picture for Langevin dynamics, with the damping constant $\gamma = 0.005$, and illustrates some mitigating effects of stochasticity.

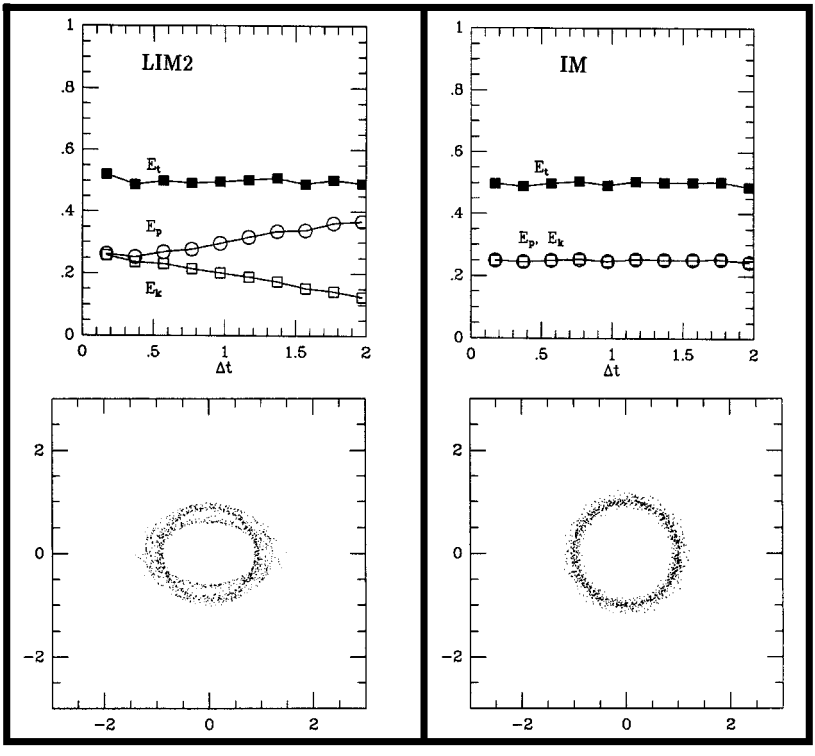

Figure 5 Harmonic oscillator average energy trends (*top*) and phase diagrams (*bottom*) as a function of timestep for two second-order, symplectic implicit integrators: LIM2 (121) (*left*) and IM (*right*) for Langevin dynamics, $\gamma = 0.005$. See Figure 4 legend, the Newtonian dynamics analogue, for other details.

We see from Figure 4 that the phase space diagrams (position, momentum) from LIM2 diverge from the expected circular shapes, and the potential energy increases while the kinetic energy decreases, as the timestep increases. In contrast, IM exhibits much better behavior for this system. The Langevin formulation (Figure 5) helps maintain better total energies for LIM2 and also reveals a spreading of the phase-space sampling for both methods.

Although IM better preserves the ratio between the potential and kinetic energy components as the timestep increases, it can accentuate resonance effects (57, 99). The analysis of a family of symplectic schemes showed that for a harmonic oscillator, IM and LIM2 display rapid divergence, as the timestep is increased, for the effective rotation in phase space (timestep and frequency

dependent) in comparison to the actual rotation value (99). This artificial, integrator-induced corruption of physical behavior was discussed above in connection with resonance. Indeed, resonance trends are most pronounced for IM.

Intrigued by resonance, Mandziuk & Schlick (57) studied resonance patterns in a nonlinear Morse oscillator. By analyzing the effective Δt-dependent IM rotation, they derived the following formula for the resonant timesteps:

$$\Delta t_{n,m} = (2/\omega_{E_t^0}) \tan(m\pi/n), \qquad n/m > 2. \tag{6}$$

In this formula, $\omega_{E_t^0}$ is a known energy-dependent angular frequency, and n and m are integers. Thus, resonance is expected for $\Delta t \approx P/2, P/3, P/4, P/5, \ldots$, where P is the period (57). The first case (third-order resonance, $n = 3, m = 1$) leads to instability, and the higher-order resonances ($n \geq 4$) lead to large energetic fluctuations and/or corrupted phase diagrams. At timesteps $\Delta t_{n,m}$ the oscillator samples n phase-space points in m revolutions and, subsequently, exhibits disconnected phase diagrams (57). Resonance patterns are illustrated in Figure 2, where according to Equation 6, with $\omega_{E_t^0} = 0.65\ \text{fs}^{-1}$, the fourth-order resonance ($n = 4$, $m = 1$) appears near 3.1 fs and the third-order resonance near 5.3 fs. Four main branches in the former, and three branches and instability in the latter can be seen. Note also the decreasing frequency of the curve oscillation as the resonant timesteps are approached.

The usefulness of this predictive formula for the resonant timesteps for nonlinear systems has not been explored thoroughly. However, current work on a dipeptide and other model systems indicates that it provides a reasonable approximation for the timestep range where resonance is expected; at the same time, it appears that nonlinear effects (e.g. van der Waals, vibrational coupling) spread the resonant regions, making it difficult to avoid them (57a). This question of resonance in symplectic integrators deserves careful attention since resonance is of general concern, particularly for symplectic integrators such as Verlet (57), and may lead to problems in MTS schemes that incorporate large timesteps for the soft interactions, close to half the period of the fastest motions. Alternatives to symplectic formulations, such as energy- and momentum-conserving schemes might work better (79), but these integrators are not yet computationally competitive.

Implicit Schemes

The implicit-Euler (IE) scheme was introduced into MD (73, 95) to maintain numerical stability for large timesteps. Since the damping of this high-stability scheme is well known, we found it necessary to use the Langevin framework to replenish the system with energy. In its simplest form, the continuous form

of the Langevin equation is given by:

$$\mathbf{M}\dot{V}(t) = -\nabla E(X(t)) - \gamma \mathbf{M} V(t) + R(t), \tag{7a}$$

$$\dot{X}(t) = V(t), \tag{7b}$$

where γ is the collision parameter and the other symbols are used as in previous equations. The random-force vector, R, is a stationary, Gaussian process with statistical properties (mean and covariances matrix) given by:

$$\langle R(t) \rangle = 0, \quad \langle R(t) R(t')^T \rangle = 2\gamma k_B T \mathbf{M} \delta(t - t'), \tag{7c}$$

where k_B is the Boltzmann constant, and δ is the usual Dirac symbol. The IE discretization of the above system was reformulated as a minimization problem for the function Φ, which contains a kinetic and potential energy term, and was then solved via a truncated-Newton minimization package (92). The resulting method was termed LI (Langevin/IE).

The energy put back via the Langevin random force in LI counteracts two damping effects: numerical—dependent on both frequency and timestep, and physical—due to friction, proportional to γ. This feature results in severe damping of the high-frequency modes, which in turn alters global motion (119, 28). However, for macroscopic models—where the high-frequency motion is absent or largely decoupled from the others—the LI method is efficient in comparison to Verlet (75, 76), allowing large-scale insights into the dynamics of supercoiled DNA modeled as an elastic material using the B-spline curve-fitting technique (77, 93).

For all-atom models, the LI framework may be used to enhance sampling and to suggest pathway information by putting back energy into the system in an ad hoc fashion. Hao et al (44) devised such a procedure based on LI and applied it to BPTI to suggest a folding pathway. Derreumaux & Schlick later developed a dynamics driver approach (DA) (28), which combines the Φ minimization of LI with configurational perturbations and incorporation of acceptance/rejection criteria in the spirit of Monte Carlo. The application of DA to a dipeptide, tetrapeptide, and an oligoalanine model demonstrated enhanced sampling and near-Boltzmann statistics for the small systems, and suggested unfolding/folding pathways for the oligoalanine (28). Current applications of DA involve the large-scale lid motion in the enzyme triosephosphate isomerase (P Derreumaux, T Schlick, & M Karplus, unpublished data).

A natural way to exploit the greater stability of implicit schemes without the damping effects of IE is to resort to a symplectic integrator. However, our applications of the IM scheme (57) revealed intriguing problems of resonance, diminishing hope for the effectiveness of related implicit symplectic methods at large timesteps (57a). Implicit methods are also costly because of the nonlinear minimization or linear-system subproblem at each timestep (121), and

they are not likely to be competitive in general. Janežič and coworkers reported such substantial increases in complexity with their implicit symplectic Runge-Kutta integrator (48), even with an efficient solution process for the resulting nonlinear system. They subsequently sought greater efficiency in parallel implementations (49) [see (55) for comments].

Currently, implicit methods do not appear competitive with other existing approaches in terms of CPU time because of the substantial cost increase of each timestep. Perhaps semi-implicit (65) or cheaper implementations of implicit schemes (RD Skeel, unpublished data) will better handle this problem by treating the local terms in an implicit manner but the nonlocal terms explicitly. This might improve the balance between the cost per timestep with the timestep increase in comparison to explicit methods. Exploitation of parallel machine architecture may provide further speed-up opportunities, though results on parallelization of linear algebra codes suggest that parallel computers may favor explicit methods.

Multiple Timestep (MTS) Methods

Even though biomolecules have a wide range of relevant timescales and motion, their potential energy can be divided into two distinct classes: internal terms—bond stretches, bond angle bends, and dihedral angles, which model the effects of covalent bonding; and external terms—van der Waals and Coulomb, which model nonbonded effects. The former class has linear complexity while the latter has an associated cost that grows quadratically with the number of atoms. The expense of calculating the external components (energy and forces) is thus especially severe when the timestep is small. This problem has stimulated more efficient approaches that exploit the more slowly varying nature of the external, in comparison to the internal, interactions.

Streett et al (102) first proposed an MTS method in which the forces were divided into fast and slow components, each of which was resolved with an appropriate timestep. The first applications of MTS used a Taylor-series extrapolation of the slow forces over a relatively long time interval, and the fast forces were evaluated at suitable (shorter) subintervals. For monoatomic molecular fluids, where no internal terms are present, distance provided the basis for the force division: nearest neighbor interactions were treated with smaller steps than distant interactions. This splitting of the external terms was continued (103) in the presence of internal terms for the simulation of chain molecules. Efficiency gains reported in the latter two works range from factors of 1.5 to 8. A group at Columbia (107) developed and applied MTS methods in a number of contexts. The work of Scully & Hermans (97) is unique in that it tests the limits of an MTS method for systems in an aqueous solution.

The modern era of MTS methods for biomolecular simulations began with the introduction of MTS variants that shared the time reversal symmetry of

the Verlet scheme. Schulten and coworkers (41) introduced the method they termed Verlet–I and, independently, Tuckerman et al (107) derived an equivalent method, *r-Respa*, by applying a Verlet variant to the Trotter factorization of the Liouville operator.

Watanabe & Karplus (115, 116) applied time reversible MTS methods to a variety of systems, including the protein BPTI, using an internal/external force splitting based on bonding topology. The Columbia group (45, 74, 122) expanded on this treatment by splitting the external forces into fast and slow parts based on distance. Since interatomic distances change over the course of a simulation, especially in aqueous environments, implementation of a switching mechanism for continuous transitions between fast- and slow-treatment zones is required.

All these studies report remarkably similar findings compared to Verlet integration with timestep $\Delta t = 0.5$ fs: MTS methods can reduce the computational work by a factor of four to five for biomolecules in vacuum while reproducing important properties of the dynamics, such as energy fluctuations and spectral densities. Reports of greater efficiency, however, should be placed more clearly in their special context. The speed-up factors of 20 or more in simulations of flexible C_{60} molecules (74) result from the succinct division of relevant timescales (i.e. intramolecular vibrations, intermolecular vibrations, and librations), allowing timesteps of up to 25 fs for the soft forces. This is not the case in biomolecules, as extensively discussed in this article. Furthermore, the speed-up factor of 20 (122) reflects the use of fast electrostatic algorithms; such schemes also apply to single-timestep methods, which should instead form the basis for MTS comparisons. Indeed, when Forester & Smith (33) incorporated a fast electrostatic treatment via Ewald sums into an MTS algorithm, they reported speed-up factors of only two to three for liquid water and a solvated protein system, in comparison to single-timestep simulations with Ewald.

Normal-Mode-Based Schemes

Normal-mode studies are useful for local analysis of protein motions (64), and much work has gone into developing efficient methods for large systems and for quasi-harmonic extensions (20, 24). The notion that essential features of macromolecules might be described by the low-frequency, high-amplitude vibrational modes has also led to the development of several interesting simulation techniques for dynamics.

Our experience with the LI scheme, which damps the high-frequency modes, led to incorporation of a normal-mode component to remedy this effect. The resulting method, termed LIN (119, 120), consists of a linearization part (a harmonic approximation to the equations of motion) and a correction part (to resolve anharmonic effects) by implicit discretization (see details in Appendix A).

The first part can be solved analytically (119), or much faster numerically (13). In (13), we showed very good agreement for dipeptide and BPTI systems simulated by LIN ($\Delta t = 30$ fs and 15 fs, respectively) in comparison with explicit Langevin simulations at the much smaller timestep of 0.5 fs. In addition, modest speed-up was realized for LIN: a factor of about 1.4 in both cases. Our variant LN emerged as a significantly more competitive method (13) since it eliminates LIN's correction step. It also gave good agreement for the systems above at 5-fs timesteps. LN is described in detail in the next subsection.

Space et al later described a subspace dynamics method (see also Reference 4) in which the low-frequency motion is propagated via a projected formulation of Newton's equations (100). The success of such a method relies on the definition and efficient computation of the low-frequency subspace. In their applications to a Lennard-Jones crystal and a glass system, Space et al found updating unnecessary, and thus the subspace was fixed at the onset of the dynamic simulation. With a sufficiently large subspace basis, results converged to the values of the reference MD trajectory, but notable deviations also emerged. Speed-up was close to the factors of timestep increases, namely 2–5, with respect to the 25-fs value used in the reference MD simulation for these systems (i.e. force calculations dominate CPU cost). In a follow-up work (7), applications to a 32-atom chain without Lennard-Jones interactions indicated that subspace calculations produce reasonable approximations. Still, results from the subspace calculation of 24 modes (out of 96) revealed significant energy damping. In general, an algorithm is needed for determining a portion of the spectrum; this is a challenging linear-algebra task in its own right. Furthermore, because of the strong vibrational coupling in biomolecules, updating the low-dimension normal-mode subspace will become necessary, and the cost of the scheme is expected to increase steeply.

A similar idea was described in a very different formalism by Janežič & Merzel (47). The same splitting mechanism of LIN (119) is employed—linearization and correction—with the high-frequency modes treated analytically by normal-mode analysis and the remaining part solved explicitly, but the symplectic implementation follows the work of Wisdom & Holman (117). From applications to the linear system $H-(C{\equiv}C)_n-H$, these researchers (47) reported an order of magnitude speed-up for the case of one harmonic approximation (held fixed throughout the simulation). For the same reasons stated above, general biomolecular applications demand frequent decomposition updating and hence increase the cost of such methods substantially. Indeed, we showed that deviations from the harmonic approximation can already occur within 15 fs (13). Only for special systems, such as those above and perhaps liquid water, clever applications of rigid-body transformations may be devised if all intermolecular and intramolecular vibrations are known a priori.

Schulten and coworkers (11) demonstrated that the principal component analysis method—related to the above notion of subspace of essential motion [see (4) and references cited in (11)]—is not suitable for describing long-time protein dynamics resulting from current simulation timespans. Essentially, although a small low-frequency subspace describes well a large fraction of the large-amplitude motions, this subspace keeps changing during the course of the simulation. Since our current nanosecond timespans are much too short relative to the longest relaxation time for proteins in aqueous environments, it is not possible to identify the essential subspace reliably. Possibly, as Amadei et al have later amended (5) their original formulation (4), enhanced sampling techniques might increase the utility of such propagation schemes.

Turner et al's (110) substructuring approach relies in part on normal modes. Hon Chun and coworkers are applying to molecular systems a technique that has been successful in aerospace dynamics: propagation of multibody dynamics modeled as a collection of rigid and flexible particles. The motion of the atoms within these bodies is propagated via their normal-mode components, of which only the lowest-frequency modes are included. The dynamics between bodies is modeled rigorously. Large overall computational gains might be possible because the number of variables is reduced dramatically (by modeling the system as a collection of large flexible bodies), and larger timesteps can be used for the flexible substructures (since the fast oscillations are absent). However, system-dependent substructuring strategies are necessary, and it is difficult to show agreement with small timestep dynamic simulations. Ultimately, such methods may succeed in capturing the slow-scale motions in biomolecules that are observed experimentally. Researchers may be able to predict slow events in macromolecules by applying artificial potentials that enhance configurational transitions (40).

The LN Algorithm

The LN method was actually formulated for diagnostic purposes, that is, to assess the range of validity of LIN's harmonic solution (13), but it emerged as a reasonable scheme on its own. Indeed, trajectories for BPTI and a dipeptide agreed with small-timestep analogues (0.5 fs) in terms of structural and energetic properties (13). Furthermore, the computational gain was promising for LN: a factor of four for BPTI (904 atoms).

The idea of LN is simple: Construct an approximation to the linearized model for the equations of motion every Δt interval (5 fs or less), and explicitly integrate this linearized system using an inner timestep $\Delta\tau$ (e.g. 0.5 fs). Since the subintegration process does not require new force evaluations, as in every step of standard MD integration, LN can be computationally efficient. To describe LN, we start from a linear approximation to the Langevin equations

(System 7) at some reference position X_r (e.g. the previous position, X^n, or the midpoint, $X^{n+1/2}$). The resulting system of equations for the harmonic approximations X and V is given by:

$$\mathbf{M}\dot{V} = -\nabla E(X_r) - \widetilde{\mathbf{H}}(X_r)(X - X_r) - \gamma \mathbf{M} V + R, \tag{8a}$$

$$\dot{X} = V, \tag{8b}$$

where the matrix $\widetilde{\mathbf{H}}$ is a sparse approximation to the Hessian of E at X_r (13), such as the Hessian resulting from the internal energy terms or from short (e.g. 4.5 Å) cutoffs. System 8 can be solved by standard NM techniques (119, 120) or alternatively can be solved numerically, at a small inner timestep $\Delta\tau$ (0.5 or 1 fs). Although in theory instability can result from vibrational modes with negative eigenvalues [complex solutions of form $\exp(-i\sqrt{\lambda}t)$], we did not find this a problem in practice over the relatively small interval of Δt used (13).

There are several possibilities for the explicit integration of System 8. If we use X^n as a reference point, an appropriate method is the second-order partitioned Runge-Kutta method (Lobatto IIIa,b) (43), which reduces to the velocity Verlet method when $\gamma = 0$. This yields the following iteration process for $\{X^{n+1}, V^{n+1}\}$ from the initial conditions $X(0) = X^n$, $V(0) = V^n$:

$$\begin{aligned}
V_{i+\frac{1}{2}} &= V_i + \frac{\Delta\tau}{2}\mathbf{M}^{-1}[-\nabla E(X_r) - \widetilde{\mathbf{H}}(X_r)(X_i - X_r) - \gamma \mathbf{M} V_{i+\frac{1}{2}} + R], \\
X_{i+1} &= X_i + \Delta\tau\, V_{i+\frac{1}{2}}, \\
V_{i+1} &= V_{i+\frac{1}{2}} + \frac{\Delta\tau}{2}\mathbf{M}^{-1}[-\nabla E(X_r) - \widetilde{\mathbf{H}}(X_r)(X_{i+1} - X_r) - \gamma \mathbf{M} V_{i+\frac{1}{2}} + R].
\end{aligned} \tag{9}$$

The first equation above is implicit for $V_{i+\frac{1}{2}}$ (the third is not for V_{i+1}), but the linear dependency in the former allows solution for $V_{i+\frac{1}{2}}$ in closed form. Note the Hessian/vector products in the first and third equations. The random force R is updated according to Equation 7c at every $\Delta\tau$ substep, so the problem of thermal equilibrium is nonexistent here (120).

Alternatively, taking X_r as the midpoint $(X^n + \frac{\Delta t}{2}V^n)$, we can define the inner iteration process of LN by:

$$\begin{aligned}
X_{i+\frac{1}{2}} &= X_i + \frac{\Delta\tau}{2}V_i, \\
V_{i+1} &= V_i + \Delta\tau\mathbf{M}^{-1} \\
&\quad \times [-\nabla E(X_r) - \widetilde{\mathbf{H}}(X_r)\,(X_{i+\frac{1}{2}} - X_r) - \gamma \mathbf{M} V_{i+1} + R], \\
X_{i+1} &= X_{i+\frac{1}{2}} + \frac{\Delta\tau}{2}V_{i+1}.
\end{aligned} \tag{10}$$

Table 2 CPU timings for BBK ($\Delta t = 0.5$ fs) and LN ($\Delta t = 3$ fs, $\Delta\tau = 0.5$ fs)[a]

Model	Atoms/ variables	$\widetilde{\mathbf{H}}$ sparsity	$T_{\widetilde{\mathbf{H}}+\nabla E}$	T_{lin}	$T_{\nabla E}$	LN T/fs	BBK T/fs	LN speed-up
BPTI	904/2712	0.012	0.48	0.03	0.38	0.177	0.76	4.29
Lysozyme	2030/6090	0.005	2.44	0.08	1.98	0.846	3.96	4.68

[a]All CPU times are given in seconds. The matrix $\tilde{\mathbf{H}}$ is formed from bond-length, bond-angle, dihedral-angle, and 1–4 electrostatic interactions. $T_{\widetilde{\mathbf{H}}+\nabla E}$ is the cost per step of evaluating both the sparse LN Hessian and the full gradient; T_{lin} is the cost per step of integrating the linear system in LN; and $T_{\nabla E}$ is the cost per step of evaluating the gradient. The CPU cost per femtosecond (T/fs) for BBK and LN is also given along with the ratio of the two (speed-up).

Therefore, the LN procedure is a dual timestep ($\{\Delta\tau, \Delta t\}$) scheme consisting of two practical tasks: (*a*) constructing the Hessian $\widetilde{\mathbf{H}}$ in Equation 8a at every Δt interval, and (*b*) solving System 8, where R is given by Equation 7c, at the timestep $\Delta\tau$ by Procedures 9 or 10. LIN continues to a correction part, detailed in Appendix A.

The cost of LN depends on several factors: the ratio $r = \Delta t/\Delta\tau$; the CPU time of evaluating $\widetilde{\mathbf{H}}$ at X_r, $T_{\widetilde{\mathbf{H}}}$; the time for evaluating the matrix/vector product $\widetilde{\mathbf{H}}d$, $T_{\widetilde{\mathbf{H}}d}$; and the time for evaluating a gradient, $T_{\nabla E}$. Specifically, let us approximate the CPU times required to cover each Δt interval by LN versus an explicit Langevin integrator, such as BBK (22). The cost of LN is dominated by $(T_{\nabla E} + T_{\widetilde{\mathbf{H}}} + rT_{\widetilde{\mathbf{H}}d})$ as opposed to $rT_{\nabla E}$ for BBK. Our results previously showed that a sparse $\widetilde{\mathbf{H}}$ resulting from 4.5-Å cutoffs evaluated every 5 fs provides similar results in comparison with explicit trajectories at 0.5 fs (13). As we show here, an even more sparse $\widetilde{\mathbf{H}}$ with only bonded interactions—bond lengths, bond angles, dihedral angles, and the 1–4 electrostatic interactions—can also be used together with a 3-fs outer timestep for similar computational gains (a factor of four or more).

Table 2 shows results for the two proteins BPTI and lysozyme. The reference timestep for the explicit Langevin integrator BBK (22) is $\Delta t = 0.5$ fs, and for LN we use $\Delta\tau = 0.5$ fs and $\Delta t = 3$ fs[4]. The Langevin bath temperature was set to T = 300 K with the collision parameter $\gamma = 20$ ps^{-1}. The CHARMM program was used for all computations (19). The initial structures were obtained from the Brookhaven Protein Data Bank. After placement of hydrogen atoms and minimization, the systems were equilibrated with 10 ps of Langevin dynamics. The LN subintegration of System 10 was used (midpoint reference), but because the gradient and Hessian of the potential energy are computed at the

[4]The reference timestep for comparisons of MTS to single-timestep methods is always the innermost timestep used; it is now generally accepted that 0.5-fs timesteps with Verlet are needed to resolve with reasonable accuracy the dynamics of biomolecules.

Table 3 Langevin dynamics averages (mean/variance) for BPTI and lysozyme simulations over 6 ps with BBK ($\Delta t = 0.5$ fs) and LN[a] ($\Delta\tau = 0.5$ fs, $\Delta t = 3$ fs) at $\gamma = 20\ \text{ps}^{-1}$

	BPTI				Lysozyme			
	BBK		LN		BBK		LN	
E^b	1622.5	33.7	1629.7	34.2	3660.3	43.8	3676.7	44.0
E_k	803.9	22.5	807.4	22.6	1818.6	32.2	1826.8	32.1
E_p^c	818.6	23.5	822.4	23.9	1841.7	32.1	1849.9	32.3
E_{bond}	321.4	14.9	321.2	14.9	714.2	21.7	714.1	21.5
E_{angle}	453.9	15.8	452.6	15.7	1009.0	24.3	1006.0	24.1
E_{tor}	352.1	8.51	354.1	8.59	725.1	11.3	729.3	11.4
E_{vdw}	−120.4	13.4	−118.7	13.6	−466.2	19.5	−462.4	19.8
E_{elec}	−1944.1	15.0	−1943.6	15.3	−4994.2	23.5	−4993.4	24.0
T^d	298.3	8.34	299.6	8.39	300.6	5.32	301.9	5.30

[a]The sparse approximate Hessian $\widetilde{\mathbf{H}}$ was constructed using bond-length, bond-angle, dihedral-angle, and 1–4 electrostatics terms.
[b]Energy is given in kcal/mol for total, kinetic, potential, bond-length, bond-angle, torsion, van der Waals, and electrostatic terms.
[c]The potential energy is given with respect to the initial values −1664.96 for BPTI and −4637.85 kcal/mol for lysozyme, corresponding to local minima near the initial configurations.
[d]Temperature is given in degrees.

point $X^{n+1/2}$, we also computed the bond and angle energy at each X^n point for reporting purposes. The added cost involved is negligible. The sparsity of $\widetilde{\mathbf{H}}$ (as described above) is the relative number of nonzeros. $T_{\widetilde{\mathbf{H}}+\nabla E}$, T_{lin}, and $T_{\nabla E}$ in the table give the cost per Δt step, respectively, of: (*a*) evaluating both the sparse Hessian and full gradient in LN, (*b*) integrating the linear system in LN, and (*c*) evaluating the full gradient in BBK. Also given is the CPU cost per fs (T/fs) for BBK and LN, and the ratio of the two (speed-up). All times are taken from 6-ps simulations in serial mode on a 194-MHz SGI R10000 Power Challenge.

We note that as system size increases (lysozyme has 2.5 times more atoms than BPTI), the number of entries in the approximate Hessian $\widetilde{\mathbf{H}}$ grows linearly, and so does the computational cost of solving the linearized equations of motion. In principle, the cost of evaluating the Hessian should also increase linearly with the number of entries. However, the current CHARMM implementation does not exploit the increased sparsity in the second-derivative calculations because of dense Hessian data structures. Still, we see an increase in the efficiency gain for larger systems, with an LN speed-up greater than a factor of four. Table 3 compares the results of LN and BBK for lysozyme and BPTI in terms of energy averages and variances. The agreement for both average energy values and variances is excellent (see (13) for further analyses).

Unlike the 4.5-Å cutoff case, the approximate Hessian $\widetilde{\mathbf{H}}$ used here does not include contributions from short-range nonbonded interactions. As a result,

all such interactions are treated as constant over the Δt interval (as is the case with traditional integrators). Smaller outer LN timesteps than those used in Reference (13) are required, but the decreased computational cost associated with the very sparse matrix yields CPU gains that compare favorably with those reported earlier. The bonded $\widetilde{\mathbf{H}}$ leads to increased efficiency in three important ways: First, the number of nonzero matrix entries is small, as is the number of operations required for matrix operations (e.g. matrix/vector products). Second, the pattern of the nonzero matrix entries, dictated by the molecular bonding topology, remains unchanged throughout the simulation, in contrast to the interaction topology for the nonbonded terms within a certain distance range, which changes dynamically. Third, the constant bonding topology also allows for simple and efficient parallel evaluation of $\widetilde{\mathbf{H}}$, which we plan to exploit in the future. We conclude that efficient Hessian treatments make possible, without sacrificing CPU gain, smaller outer timesteps in LN, which result in more accurate trajectories.

Several important issues remain to be explored in connection with LN. These involve the best general choices for $\widetilde{\mathbf{H}}$ that balance both physical and computational performance; the best choice for the LN outer timestep value (probably system dependent and smaller for larger systems, but the incorporation of adaptive timestep selection or extrapolation techniques might allow larger timesteps); implementation of clever sorting and computational tricks to improve the efficient handling of sparse Hessians; applications to biomolecules in solution, where intermolecular collisions (when water is modeled explicitly) might cause problems; a more general assessment of the Langevin vs Newtonian dynamics approach and examination of LN's configurational sampling capabilities. Currently, we are combining the force linearization idea of LN with the force splitting idea of MTS methods; the speed-ups are significant (E Barth & T Schlick, in preparation).

SOME COMPARATIVE NUMERICAL EXPERIMENTS

To gain insight into the behavior of the various MD algorithms described in the previous section, we performed comparative experiments on the alanine dipeptide system (shown in Figure 1) within the CHARMM program (19). The dipeptide is sufficiently small for algorithmic experimentation yet is also interesting physically because of its flexibility. We compared methods in two classes: Newtonian dynamics and Langevin dynamics. For the first, we used the following four integration schemes and associated timesteps: leap-frog/Verlet (LF) with $\Delta t = 0.5$ fs; a dual-timestep MTS method with $\Delta t_1 = 0.5$ fs and $\Delta t_2 = 2.5$ fs (116); a SHAKE model with constraints only on bonds to hydrogen atoms (CON1) with $\Delta t = 2$ fs; and a SHAKE model with all bonds plus

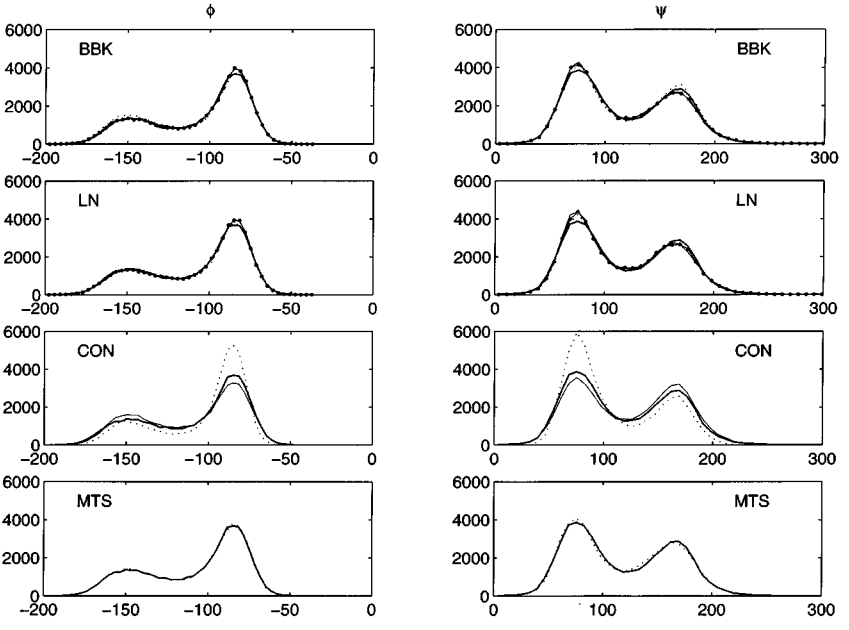

Figure 6 Alanine dipeptide distributions of the torsion angles $\{\phi, \psi\}$, in degrees, for various methods as obtained from 3-ns trajectories. Thick lines give results for LF in each view. For BBK and LN, results for three γ (in ps^{-1}) are also shown: $\gamma = 5$ (*thin line*), $\gamma = 20$ (*line with large dots*), and $\gamma = 50$ (*dots*). For the constrained methods, results are given for CON1 (*thin line*) and CON2 (*dots*).

bond angles involving hydrogen atoms constrained (CON2) with $\Delta t = 4$ fs. In CON1, constraints were made to the equilibrium values, and in CON2 variables were constrained to the initial simulation values. For Langevin dynamics, we compared, at three γ values, BBK to LN results. BBK is the Verlet generalization to stochastic dynamics (22). For BBK, we used $\Delta t = 0.5$ fs, and for LN $\Delta\tau = 0.5$ fs and $\Delta t = 5$ fs. Each trajectory was started from the same initial conditions—obtained following a 160-ps equilibration at 300 K beginning at the C7 equatorial minimum (54)—and, for the stochastic methods, the same random seed was used in all cases. The dihedral-angle data were generated from points along the trajectory at 60-fs intervals.

Results are summarized by ϕ and ψ distributions in Figure 6 and $\{\phi, \psi\}$ phase diagrams in Figure 7. Each window of Figure 6 shows the LF results as a reference (solid lines). For the stochastic simulations, three additional curves correspond to the γ used: 5, 20, and 50 ps^{-1}. Overall, the Langevin simulations give distributions similar to LF. More rigid behavior (sharper peaks) is observed

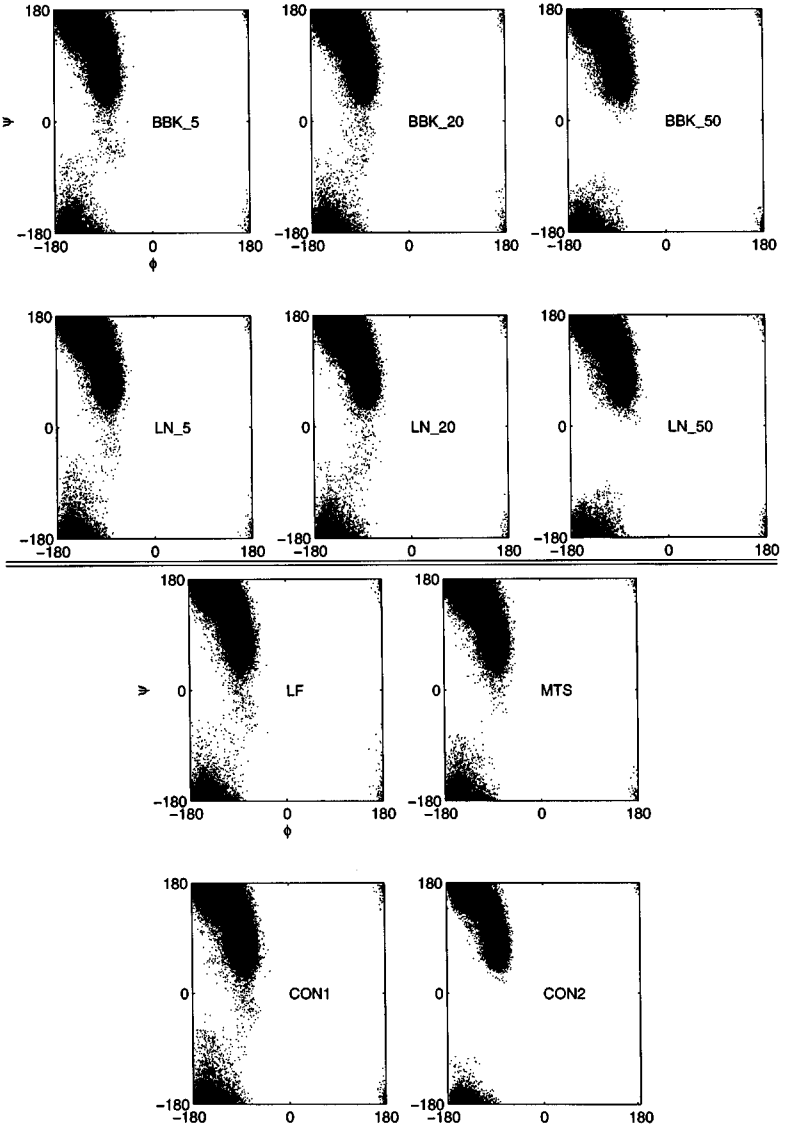

Figure 7 Alanine dipeptide $\{\phi, \psi\}$ phase diagrams, in degrees, for the various methods generated from coordinates taken every 60 fs from 3-ns trajectories. The numbers following the method name indicate the γ value used for BBK and LN.

for both BBK and LN for the largest γ. The MTS method and the procedure of constraints CON1 also match the results of LF well, though larger differences are evident for MTS (see sparser phase diagram). A substantial difference is evident for CON2 resulting from the additional constraints used (heavy-atom bond stretches and light-atom bends). The results of LN agree excellently with BBK, as seen from both the distributions and phase diagrams.

Langevin vs Newtonian Dynamics

The Langevin framework can be used both for numerical stabilization (121) and enhanced sampling (28, 54). Recall that figures 4 and 5 reveal the energy-stabilizing influence of the stochastic terms for the symplectic integrator LIM2 (121) and the spreading of phase diagrams in the Langevin framework. For the alanine dipeptide, a nonzero γ can be chosen for optimal sampling, although too large a value can inhibit sampling due to the smaller relative contribution of the inertial terms (71). We did not observe any significant advantages in sampling for the dipeptide over the 3-ns interval sampled here, but a much quicker equilibration time was found to be advantageous in the Langevin simulations.

The size of fluctuations in total energy has been used widely in the literature to assess the quality of MD methods. This concept is meaningful only in the constant-energy Newtonian simulations. From Table 4, we see that the fluctuations in total energy for the stochastic methods are larger than for the Verlet and the constrained methods, but significantly, fluctuations of the internal variables are nearly identical. Averages and fluctuations of the individual energy components agree well.

Constraints

We noted in our discussion of Figure 1 that constraining bonds to hydrogen atoms eliminates the fastest regions of the vibrational spectrum and that adding heavy-atom bond constraints achieves small gains. The smaller number of bonds with light atoms for the dipeptide (12 out of 21) and the simple bond topology ensure rapid convergence when solving the constrained formulation for the light bonds only. However, constraining all bonds is inefficient because computations increase at each timestep, while the timestep cannot be increased because of the overlap of frequencies associated with light-atom bends and heavy-atom stretches (Figure 1).

Constraining all bonds plus light-atom angles can eliminate another frequency peak (Figure 1) and hence increases the feasible timestep. Indeed, a timestep of 4 fs is used in CON2 as opposed to 2 fs in CON1. However, as results from the corresponding CON2 procedure indicate in Figures 6 and 7 and Table 4, the overall motion of the molecule is more restricted. Further, from the CPU timings in Table 4 (last row), we see that although the timestep is increased by a factor of eight (from 0.5 fs) in reference to LF, the overall

Table 4 Averages (mean/variance) for alanine dipeptide, from 3-ns trajectories produced by various methods

	LF[a] [$\Delta t = 0.5$ fs]		BBK[b] [$\Delta t = 0.5$ fs] $\gamma = 5$, $\gamma = 20$, $\gamma = 50$ ps^{-1}		LN[c] [$\Delta\tau = 0.5$ fs $\Delta t = 5$ fs] $\gamma = 5$, $\gamma = 20$, $\gamma = 50$ ps^{-1}		CON1[d] [$\Delta t = 2$ fs]		CON2[e] [$\Delta t = 4$ fs]		MTS[f] [$\Delta t_1 = 0.5$ fs, $\Delta t_2 = 2.5$ fs]	
			21.4	4.74	21.3	4.90						
E^g	19.5	0.021	21.5	4.74	21.7	4.87	15.5	0.118	8.79	0.074	19.5	0.053
			21.4	4.75	21.6	4.85						
			19.6	3.42	19.7	3.48						
E_k	17.8	2.27	19.7	3.42	19.8	3.47	15.6	2.22	6.036	1.34	17.8	2.27
			19.7	3.43	19.6	3.44						
			1.73	3.28	1.57	3.22						
E_p	1.67	2.28	1.78	3.28	1.89	3.35	−0.033	2.31	2.75	1.39	1.73	2.29
			1.77	3.28	1.95	3.35						
			299.5	52.1	300.8	53.1						
T^h	299.2	38.1	300.1	52.1	301.9	52.9	326.4	46.5	303.8	67.8	298.1	38.1
			300.1	52.3	299.4	52.4						
			6.72	2.07	6.56	2.06						
E_{bond}	6.57	1.86	6.73	2.07	6.73	2.07	3.52	1.57	0.00	0.00	6.70	1.87
			6.73	2.07	6.71	2.06						
			8.89	2.37	8.78	2.35						
E_{angle}	8.92	2.16	8.91	2.38	8.80	2.35	9.79	2.32	8.86	1.63	8.80	2.14
			8.88	2.37	8.82	2.35						
			4.71	1.02	4.72	1.01						
E_{tor}	4.69	1.02	4.71	1.02	4.75	1.03	4.80	1.09	4.86	1.11	4.71	1.02
			4.70	1.03	4.78	1.05						

			−106.4	29.9	−106.3	29.8						
ϕ[i]	−107.5	30.3	−107.0	30.3	−106.8	30.1	−110.5	31.2	−103.1	28.0	−107.4	30.3
			−109.1	31.2	−108.1	30.7						
			116.3	47.9	115.9	47.8						
	118.1	48.5	117.5	48.5	117.1	47.7	123.1	49.4	108.6	42.6	117.8	47.5
			118.9	47.1	118.1	46.3						
			1.53	0.034	1.53	0.034						
$^{r}C_{\alpha}C$[j]	1.53	0.034	1.53	0.034	1.53	0.034	1.53	0.036	1.50	0.0	1.53	0.034
			1.53	0.034	1.53	0.034						
			123.3	3.26	123.3	3.22						
$^{\theta}CNC_{\alpha}$ [h]	123.3	3.30	123.3	3.28	123.3	3.27	123.3	3.46	122.2	3.06	123.3	3.25
			123.3	3.29	123.2	3.28						
			110.8	4.10	110.8	4.09						
$^{\theta}NC_{\alpha}C$	110.7	4.10	110.8	4.12	110.8	4.11	110.5	4.30	112.6	4.07	110.7	4.10
			110.6	4.15	110.7	4.13						
			117.0	2.80	117.0	2.77						
$^{\theta}C_{\alpha}CN$	117.0	2.80	117.0	2.76	117.0	2.76	117.0	2.95	117.4	2.78	117.0	2.77
			117.0	2.77	117.0	2.76						
CPU	1.0		1.0		0.48		0.29		0.50		0.42	

[a] Leap-frog/Verlet (LF) (3).
[b] Verlet version for Langevin dynamics (22).
[c] The Langevin/Normal Mode scheme described here (13).
[d] All light-atom bonds constrained via SHAKE (87).
[e] All bonds and light-atom bends constrained via SHAKE and implemented by an iterative Newton scheme (12).
[f] A multiple-timestep method offered in CHARMM (116).
[g] Energy is given in kcal/mol; see Table 3 for components.
[h] Temperature is given in degrees.
[i] Angles are measured in degrees.
[j] Bond lengths are given in Ångstrom.

gain in efficiency is only about a factor of two (40 constraints used: 21 bonds and 25 bond angles). More generally, even though the computational overhead of solving for the constraints would likely decrease with larger systems, the decreased flexibility is a drawback to this approach. The CON1 procedure appears to be the winner on both physical and computational grounds.

Performance of LN

The LN method emerges well from these comparisons. Table 4 shows that LN agrees well with BBK. Since it is a Langevin dynamics method, LN also offers the possibility of faster conformational sampling than Newtonian dynamics. The linearization approximation over each 5-fs interval appears reasonable, and the subintegration process is fast.

Computational Efficiency

The last row of Table 4 reports for the dipeptide simulations the observed cost per unit time for each method relative to the cost of LF (or BBK) at $\Delta t = 0.5$ fs, which requires one force evaluation per step. For LN, the timing was performed using CHARMM version 24b1 on an SGI Indigo2 workstation; for CON2, CHARMM version 23f4 was used on the Indigo2; all other timings were taken from simulations using CHARMM 24b1 on an SGI Power Challenge running in serial mode. Timing data for LF/BBK were obtained on each machine and for each CHARMM version as well, so that fair comparisons could be made independent of implementation. For the constrained CON1 method, since the timestep is 2 fs (four times larger than the reference simulation), the asymptotic speed-up is four and corresponds to the relative time of 0.25; thus, near-peak speed-up is already observed for the dipeptide, and similar speed-ups should be obtained for larger systems if the constraints are handled efficiently. For the constrained CON2 method, the asymptotic speed-up of eight (from the 4 fs timestep) is not observed because of the relatively large number of constraints for this small system. However, CON2 is not recommended for physical considerations, as shown by the effects of these constraints on the torsion-angle motion (Figures 6 and 7).

The LN and MTS methods gain efficiency for large systems, as the ratio of nonbonded to bonded interactions increases. Since the small dipeptide has approximately 25% bonded interactions, the MTS scheme cannot reach its expected speed-up of five with the outer timestep of 2.5 fs (i.e. relative CPU value of 0.2) and LN cannot reach its asymptotic (but not expected) speed-up of ten (CPU value of 0.1). The LN speed-up here of about two, as demonstrated in (13) can be improved for larger systems when a sparse $\widetilde{\mathbf{H}}$ is used (as discussed in the last section and in Table 2), since sparsity increases rapidly with system size (29). For larger systems, a speed-up factor of four or more is possible

for both methods (see (45) for MTS, and Table 2 and (13) for LN), and LN combined with force splitting improves on this factor (E Barth & T Schlick, in preparation).

PERSPECTIVES

This review has surveyed some of the exciting algorithmic activities focusing on increasing the timestep and hence the timespan of all-atom biomolecular simulations. Many innovative techniques ranging from brute force to approximate dynamics propagators have been developed. Long-timestep integration is particularly challenging when strictly faster methods with the same all-atom resolution of small-timestep trajectories are sought. Because of the strong vibrational coupling in biomolecules, mathematical techniques that exploit mode separation or the rapid decay of the fast motions in multiple-timescale systems have not been directly applicable to molecular dynamics. Indeed, progress in increasing the timespan covered by all-atom biomolecular simulations has been slow relative to improvements in computer power during the past decade.

The approaches described here (constrained and torsion dynamics, implicit and symplectic schemes, MTS methods, and normal-mode-based schemes) aim at generating continuous dynamics and attempt to balance reliability of the results—as compared to small-timestep simulations—with computational advantages. This task is more difficult for methods that substantially increase the timestep, since the work per step generally increases and some local motion is approximated. Constrained formulations combined with explicit integration presently yield modest computational gains and, as shown here, constraining the light-atom bonds can yield the near-asymptotic speed-up corresponding to the timestep increase. Other methods that yield modest speed-up but are somewhat more complex to implement are MTS methods and the LN scheme. Both require careful testing and possible further development in aqueous environments and in the presence of fast electrostatic treatments; the inclusion of explicit water molecules increases the ratio of fast interactions and also increases intermolecular collisions, which influence numerical behavior. Straightforward implicit discretization schemes are probably too costly, though parallel implementations may help reduce the added costs per step. Torsion-angle dynamics approaches appear most useful for enhanced sampling at elevated temperatures, and various methods based on the essential subspace concept are likely to be useful only in combination with efficient sampling techniques.

A broader view should also lead to a heightened appreciation of methods that approximate dynamical fluctuations but that can cover much more configurational space. These methods include hybrid Monte Carlo/MD techniques,

simulations with macroscopic models, incorporation of available experimental data, and possibly artificial potential terms to guide the system along a certain path.

An interesting new approach is a path optimization algorithm based on the stochastic path integral of Onsager and Machlup (31, 70). Trajectories between two given end points are generated at a relatively large timestep by an optimization procedure (conjugate gradient, simulated annealing, or multigrid techniques). Numerical stability is achieved because the high-frequency motions that cannot be resolved at the chosen timestep are filtered out automatically. In addition, an error estimate of the filtered motions can be obtained. Numerical experiments on a double-well potential and an alanine dipeptide system (70) reveal the stability and filtering capabilities of the method, as well as its ability to find paths between two states of biological interest. The method is expensive at present, and techniques for complete relaxation along the pathway require further development; however, the suggestion of long-time dynamics behavior is encouraging.

Another area of great potential that is natural for macromolecular simulations involves multigrid (or multiscale) techniques, well-known tools in applied mathematics (91). These methods solve large and complex problems efficiently by dividing the solution process among various levels of spatial and temporal resolution recursively so as to minimize computations on the the finest scale without an overall sacrifice in accuracy. MTS schemes and fast multipole treatments are two examples of multiscale techniques, and others will undoubtedly emerge.

Overall, a hierarchy of models and methods for continuous dynamics as well as conformational sampling, combined with accelerated performance on parallel architectures and improvements in experimentational resolution, are essential to give theoretical modeling the status of partner with experiment. An exciting era of association between theory and experiment is on the horizon.

ACKNOWLEDGMENTS

We are grateful to Bernie Brooks, Ron Elber, Jan Hermans, Dusanka Janežič, Martin Karplus, Andy McCammon, Sebastian Reich, Harold Scheraga, Klaus Schulten, Bob Skeel, Mark Tuckerman, and Wilfred van Gunsteren for sharing their recent work, and to Kevin Young for preparing two figures. We also thank Jan Hermans and Bob Skeel for critical reading of the manuscript. Research support from the National Institutes of Health (Parallel Computing Resource for Structural Biology award RR08102), the National Science Foundation (Grand Challenge Award ASC-9318159), and the Alfred P. Sloan Foundation is gratefully acknowledged. T.S. is an investigator of the Howard Hughes Medical Institute.

APPENDIX A: OUTLINE OF LIN

To define the LIN algorithm, we express the collective position vector of the system as $X(t) = X_h(t) + Z(t)$. (In LN, $Z(t)$ is zero.) The first part of LIN is the solution of the linearized Langevin equation for the harmonic component of the motion, $X_h(t)$ by Systems 9 or 10. The second part relies on implicit integration to compute the residual component, $Z(t)$, with a large timestep.

Specifically, once $X_h(t)$ is obtained numerically as a solution to System 8, the residual motion component, $Z(t)$, can be determined by solving the new set of equations that Z satisfies. These equations are determined by using $Z = X - X_h$ and the origin of X and X_h as solutions of Systems 7 and 8, respectively (119). This leads to:

$$\mathbf{M}\dot{W}(t) = -\nabla E(X_h + Z(t)) - \gamma \mathbf{M} W(t) + \nabla E(X_r(t)) + \widetilde{\mathbf{H}}(X_h - X_r), \tag{A.1a}$$

$$\dot{Z}(t) = W(t). \tag{A.1b}$$

Here W denotes the time derivative of Z, and the initial conditions for System A.1 are: $Z(0) = 0$ and $W(0) = 0$.

To solve System A.1, we apply to it the second-order midpoint scheme (see System 3) and follow the same algebraic manipulation outlined in References 119 and 120 to produce a nonlinear system $\nabla\Phi(Y) = 0$, where $Y = (X + X^n)/2$. This system can be solved by reformulating the problem as a minimization one for the dynamics function Φ:

$$\Phi(Y) = 2\left(1 + \frac{\gamma\Delta t}{2}\right)\left(Y - Y_0^n\right)^T \mathbf{M}\left(Y - Y_0^n\right) + (\Delta t)^2 E(Y), \tag{A.2}$$

$$Y_0^n = \frac{(X_h^{n+1} + X^n)}{2} + \frac{(\Delta t)^2}{4(1 + \frac{\gamma\Delta t}{2})}\mathbf{M}^{-1} \times \left[\nabla E(X_r) + \mathbf{H}_h\left(\frac{X_h^{n+1} + X^n}{2} - X_r\right)\right]. \tag{A.3}$$

Thus, each correction step of LIN requires nonlinear minimization of Φ, which can be accomplished efficiently using our truncated Newton package (29, 92, 94). The initial approximate minimizer of Φ can be X_h^{n+1} or $(X_h^{n+1} + X^n)/2$ (we use the latter). The new coordinate and velocity vectors for timestep $n+1$ are then obtained from the relations

$$X^{n+1} = 2Y - X^n, \quad V^{n+1} = V_h^{n+1} + 2\left(X^{n+1} - X_h^{n+1}\right)/\Delta t. \tag{A.4}$$

Literature Cited

1. Abagyan RA, Totrov M. 1994. Biased probability Monte Carlo conformational searches and electrostatic calculations for peptides and proteins. *J. Mol. Biol.* 235:983–1002
2. Abagyan RA, Mazur AK. 1989. New methodology for computer-aided modelling of biomolecular structure and dynamics: 2. Local deformations and cycles. *J. Biomol. Struct. Dyn.* 6:833–45
3. Allen MP, Tildesley DJ. 1990. *Computer Simulation of Liquids.* New York: Oxford Univ. Press
4. Amadei A, Linssen ABM, Berendsen HJC. 1993. Essential dynamics of proteins. *Proteins Struct. Funct. Gen.* 17:412–25
5. Amadei A, Linssen ABM, deGroot BL, van Aalten DMF, Berendsen HJC. 1996. An efficient method for sampling the essential subspace of proteins. *J. Biomol. Struct. Dyn.* 13:615–25
6. Andersen H. 1983. Rattle: a 'velocity' version of the SHAKE algorithm for molecular dynamics calculations. *J. Comput. Phys.* 52:24–34
7. Askar A, Space B, Rabitz H. 1995. Subspace method for long time scale molecular dynamics. *J. Phys. Chem.* 99:7330–38
8. Auffinger P, Louise-May S, Westhof E. 1995. Multiple molecular dynamics simulations of the anticodon loop of $rRNA^{Asp}$ in aqueous solution with counterions. *J. Am. Chem. Soc.* 117:6720–26
9. Auffinger P, Louise-May S, Westhof E. 1996. Molecular dynamics simulations of the anticodon hairpin of $tRNA^{Asp}$. Structuring effects of C–H···O hydrogen bonds and long-range hydration forces. *J. Am. Chem. Soc.* 118:1181–89
10. Bae DS, Haug EJ. 1987. A recursive formulation for constrained mechanical system dynamics: Part I. Open loop systems. *Mech. Struct. Mach.* 15:359–82
11. Balsera MA, Wriggers W, Oono Y, Schulten K. 1996. Principal component analysis and long time protein dynamics. *J. Phys. Chem.* 100:2567–72
12. Barth E, Kuczera K, Leimkuhler B, Skeel RD. 1995. Algorithms for constrained molecular dynamics. *J. Comput. Chem.* 16:1192–1209
13. Barth E, Mandziuk M, Schlick T. 1997. A separating framework for increasing the timestep in molecular dynamics. In *Computer Simulation of Biomolecular Systems: Theoretical and Experimental Applications*, ed. WF van Gunsteren, PK Weiner, AJ Wilkinson, Chapter 4. Leiden, The Netherlands: ESCOM.
14. Berens PH, Mackay DH, White GM, Wilson KR. 1983. Thermodynamics and quantum corrections from molecular dynamics for liquid water. *J. Chem. Phys.* 79:2375–89
15. Biesiadecki JJ, Skeel RD. 1993. Dangers of multiple-time-step methods. *J. Comput. Phys.* 109:318–28
16. Board JA Jr, Kalé LV, Schulten K, Skeel RD, Schlick T. 1994. Modeling biomolecules: larger scales, longer durations. *IEEE Comput. Sci. Eng.* 1:19–30
17. Bornemann FA, Schütte C. 1995. A mathematical approach to smoothed molecular dynamics: correcting potentials for freezing bond angles. *Tech. Rep. SC 95-30 Konrad-Zuse-Zentrum für Informationstechnik Berlin*
18. Brass A, Pendleton BJ, Chen Y, Robson B. 1993. Hybrid Monte Carlo simulations theory and initial comparison with molecular dynamics. *Biopolymers* 33:1307–15
19. Brooks BR, Bruccoleri RE, Olafson BD, States DJ, Swaminathan S, Karplus M. 1983. CHARMM: a program for macromolecular energy, minimization, and dynamics calculations. *J. Comput. Chem.* 4:187–217
20. Brooks BR, Janežič D, Karplus M. 1995. Harmonic analysis of large systems. I. Methodology. *J. Comput. Chem.* 16:1522–42
21. Brooks CL III, Karplus M, Pettitt BM. 1988. *Proteins: A Theoretical Perspective of Dynamics, Structure, and Thermodynamics, Advances in Chemical Physics* LXXI. New York: Wiley
22. Brünger AT, Brooks CL III, Karplus M. 1982. Stochastic boundary conditions for molecular dynamics simulations of ST2 water. *Chem. Phys. Lett.* 105:495–500
23. Brünger AT, Rice LM. 1995. Simulated annealing applied to crystallographic structure refinement. In *Adaption of Simulated Annealing to Chemical Optimization Problems*, ed. JH Kalivas, pp. 259–80. Amsterdam, The Netherlands: Elsevier
24. Case DA. 1994. Normal mode analysis of protein dynamics. *Curr. Opin. Struct. Biol.* 4:385–90
25. Channell PJ, Scovel C. 1990. Symplectic integration of Hamiltonian systems. *Nonlinearity* 3:231–59

26. Dahlquist G, Björck Å. 1974. *Numerical Methods.* Englewood Cliffs, NJ: Prentice Hall
27. Daura X, Oliva B, Querol E, Avilés FX, Tapia O. 1996. On the sensitivity of MD trajectories to changes in water-protein interaction parameters: the potato carboxypeptidase inhibitor in water as a test case for the GROMOS force field. *Proteins Struct. Funct. Gen.* 25:89–103
28. Derreumaux P, Schlick T. 1995. Long-time integration for peptides by the dynamics driver approach. *Proteins Struct. Funct. Gen.* 21:282–302
29. Derreumaux P, Zhang G, Brooks B, Schlick T. 1994. A truncated-Newton method adapted for CHARMM and biomolecular applications. *J. Comput. Chem.* 15:532–52
30. Duane S, Kennedy AD, Pendleton BJ, Roweth D. 1987. Hybrid Monte Carlo. *Phys. Lett. B* 195:216–22
31. Elber R. 1996. Novel methods for molecular dynamics simulations. *Curr. Opin. Struct. Biol.* 6:232–35
32. Elofsson A, Nilsson L. 1991. How consistent are molecular dynamics simulations? Comparing structure and dynamics in reduced and oxidized *Escherichia coli* thioredoxin. *J. Mol. Biol.* 233:766–80
33. Forester T, Smith W. 1994. On multiple time-step algorithms and the Ewald sum. *Mol. Simul.* 13:195–204
34. Forrest BM, Suter UW. 1994. Hybrid Monte Carlo simulations of dense polymer systems. *J. Chem. Phys.* 101:2616–19
35. Gear CW. 1971. *Numerical Initial Value Problems in Ordinary Differential Equations.* Englewood Cliffs, NJ: Prentice Hall
36. Gibson KD, Scheraga H. 1990. Variable step molecular dynamics: an exploratory technique for peptides with fixed geometry. *J. Comput. Chem.* 11:468–86
37. Goldstein H. 1980. *Classical Mechanics.* Reading MA, Addison-Wesley
38. Gray SK, Noid DW, Sumpter BG. 1994. Symplectic integrators for large scale molecular dynamics simulations: a comparison of several explicit methods. *J. Chem. Phys.* 101:4062–72
39. Grønbech-Jensen N, Doniach S. 1994. Long time overdamped Langevin dynamics of molecular chains. *J. Comput. Chem.* 15:997–1012
40. Grubmüller H. 1995. Predicting slow structural transitions in macromolecular systems: conformational flooding. *Phys. Rev. E* 52:2893–906
41. Grubmüller H, Heller H, Windemuth A, Schulten K. 1991. Generalized Verlet algorithm for efficient molecular dynamics simulations with long-range interactions. *Mol. Simul.* 6:121–42
42. Hairer E, Nørsett SP, Wanner G. 1993. *Solving Ordinary Differential Equations. I. Nonstiff Problems. Springer Ser. Comput. Math.* 8. New York: Springer-Verlag
43. Hairer E, Wanner G. 1991. *Solving Ordinary Differential Equations II. Stiff and Differential-Algebraic Problems. Springer Ser. Comput. Math.* 14. New York: Springer-Verlag
44. Hao MH, Pincus MR, Rackovsky S, Scheraga HA. 1993. Unfolding and refolding of the native structure of bovine pancreatic trypsin inhibitor studied by computer simulations. *Biochemistry* 32:9614–31
45. Humphreys DE, Friesner RA, Berne BJ. 1994. A multiple-time-step molecular dynamics algorithm for macromolecules. *J. Phys. Chem.* 98:6885–92
46. Hünenberger PH, Mark AE, van Gunsteren WF. 1995. Computational approaches to study protein unfolding: hen egg white lysozyme as a case study. *Proteins Struct. Funct. Gen.* 21:196–213

46a. Jian H, Vologodskii A, Schlick T. 1996. A combined wormlike chain and bead model for dynamic simulations of long DNA. *J. Comp. Phys.* Submitted

47. Janežič D, Merzel F. 1995. An efficient symplectic integration algorithm for molecular dynamics simulations. *J. Chem. Inf. Comput. Sci.* 35:321–26
48. Janežič D, Orel B. 1993. Implicit Runge-Kutta method for molecular dynamics integration. *J. Chem. Inf. Comput. Sci.* 33:252–57
49. Janežič D, Orel B. 1994. Parallelization of an implicit Runge-Kutta method for molecular dynamics integration. *J. Chem. Inf. Comp. Sci.* 34:641–46
50. Kang F. 1985. On difference schemes and symplectic geometry. In *Proc. 1984 Beijing Symp. Differential Geometry and Differential Equations-Computation of Differential Equations*, ed. F Kang, pp. 42–58. Beijing: Science Press
51. Kang F. 1990. The Hamiltonian way for computing Hamiltonian dynamics. In *Applied and Industrial Mathematics*, ed. R Spigler, pp. 17–35. Dordrecht, The Netherlands: Kluwer Academic
52. Leimkuhler B, Skeel RD. 1994. Symplectic numerical integrators in constrained Hamiltonian systems. *J. Comput. Phys.* 112:117–25
53. Leimkuhler BJ, Reich S, Skeel RD. 1996. Integration methods for molecular

dynamics. In *Mathematical Approaches to Biomolecular Structure and Dynamics*, ed. JP Mesirov, K Schulten, DW Sumners. *IMA Vol. Math. Appl.* 82:161–86. New York: Springer-Verlag
54. Loncharich RJ, Brooks BR, Pastor RW. 1992. Langevin dynamics of peptides: the frictional dependence of isomerization rates of N-acetylalanyl-N′-methylamide. *Biopolymers* 32:523–35
55. López-Marcos M, Sanz-Serna JM, Díaz JC. 1996. Are Gauss-Legendre methods useful in molecular dynamics? *J. Comput. Appl. Math.* 67:173–79
56. Ludovice PJ, Suter UW. 1991. Molecular dynamics of geometrically constrained polymer systems in generalized coordinates: basic formalism. *Comput. Polym. Sci.* 1:69–79
57. Mandziuk M, Schlick T. 1995. Resonance in the dynamics of chemical systems simulated by the implicit-midpoint scheme. *Chem. Phys. Lett.* 237:525–35

57a. Mandziuk M, Schlick T, Skeel RD, Srinivas K. 1997. Nonlinear resonance artifacts in molecular dynamics simulations. In preparation

58. Manolopoulos DE, Gray SK. 1995. Symplectic integrators for the multichannel Schrödinger equation. *J. Chem. Phys.* 102:9214–27
59. Marple SL. 1987. *Digital Spectral Analysis with Applications.* Englewood Cliffs, NJ: Prentice-Hall
60. Martyna GJ, Tuckerman ME. 1995. Symplectic reversible integrators: predictor-corrector methods. *J. Chem. Phys.* 102:8071–77
61. Martyna GJ, Tuckerman ME, Tobias DJ, Klein ML. 1996. Explicit reversible integrators for extended systems dynamics. *Mol. Phys.* 87:1117–57
62. Mazur AK, Abagyan RA. 1989. New methodology for computer-aided modeling of biomolecular structure and dynamics: 1. Non-cyclic structures. *J. Biomol. Struct. Dyn.* 6:815–32
63. Mazur AK, Dorofeev VE, Abagyan RA. 1991. Derivation and testing of explicit equations of motion for polymers described by internal coordinates. *J. Comput. Phys.* 92:261–72
64. McCammon JA, Harvey SC. 1987. *Dynamics of Proteins and Nucleic Acids.* Cambridge, MA: Cambridge Univ. Press
65. McCammon JA, Pettitt BM, Scott LR. 1994. Ordinary differential equations of molecular dynamics. *Comput. Math. Appl.* 28:319–26
66. McLachlan RI, Atela P. 1992. The accuracy of symplectic integrators. *Nonlinearity* 5:541–62
67. Mishra B, Schlick T. 1996. The notion of error in Langevin dynamics: 1. Linear analysis. *J. Chem. Phys.* 105:299–318
68. Miyamoto S, Kollman PA. 1992. SETTLE: an analytical version of the SHAKE and RATTLE algorithm for rigid water models. *J. Comput. Chem.* 13:952–62
69. Nyberg A, Schlick T. 1992. Increasing the time step in molecular dynamics. *Chem. Phys. Lett.* 198:538–46
70. Olender R, Elber R. 1996. Calculation of classical trajectories with a very large time step: formalism and numerical examples. *J. Chem. Phys.* 105:9299–315
71. Pastor RW. 1994. Techniques and applications of Langevin dynamics simulations. In *The Molecular Dynamics of Liquid Crystals*, ed. GR Luckhurst, CA Veracini, pp. 85–138. Dordrecht, The Netherlands: Kluwer Academic
72. Pastor RW, Brooks BR, Szabo A. 1988. An analysis of the accuracy of Langevin and molecular dynamics algorithms. *Mol. Phys.* 65:1409–19
73. Peskin CS, Schlick T. 1989. Molecular dynamics by the backward Euler's method. *Commun. Pure Appl. Math.* 42:1001–31
74. Procacci P, Berne BJ. 1994. Computer simulations of solid C_{60} using multiple time-step algorithms. *J. Chem. Phys.* 101:2421–31
75. Ramachandran G, Schlick T. 1995. Solvent effects on supercoiled DNA dynamics explored by Langevin dynamics simulations. *Phys. Rev. E* 51:6188–203
76. Ramachandran G, Schlick T. 1996. Beyond optimization: simulating the dynamics of supercoiled DNA by a macroscopic model. In *Global Minimization of Nonconvex Energy Functions: Molecular Conformation and Protein Folding*, ed. PM Pardalos, D Shalloway, G Xue. *DIMACS Ser. Discrete Math. Theor. Comput. Sci.* 23:215–31. Providence, RI: Am. Math. Soc.
77. Ramachandran G, Schlick T. 1997. Buckling transitions in superhelical DNA: dependence on the elastic constants and DNA size. *Biopolymers* 41:5–25
78. Reich S. 1995. Smoothed dynamics of highly oscillatory Hamiltonian systems. *Physica D* 89:28–42
79. Reich S. 1996. Enhancing energy conserving methods. *BIT* 36:122–34
80. Reich S. 1996. Symplectic integration of constrained Hamiltonian systems by

composition methods. *SIAM J. Numer. Anal.* 33:475–91
81. Reich S. 1996. Torsion dynamics of molecular systems. *Phys. Rev. E* 53:4176–81
82. Reiter C. 1995. Forecast: clear weather ahead. *Northwest. Perspect.* Winter 23–24
83. Rice LM, Brünger AT. 1994. Torsion angle dynamics: reduced variable conformational sampling enhances crystallographic structure refinement. *Proteins Struct. Funct. Gen.* 19:277–90
84. Rubin H, Ungar P. 1957. Motion under a strong constraining force. *Commun. Pure Appl. Math.* 10:65–87
85. Ruth RD. 1983. A canonical integration technique. *IEEE Trans. Nucl. Sci.* 30:2669
86. Ryckaert JP, Bellemans A. 1975. Molecular dynamics of liquid n-butane near its boiling point. *Chem. Phys. Lett.* 30:123–25
87. Ryckaert JP, Ciccotti G, Berendsen HJC. 1977. Numerical integration of the Cartesian equations of motion of a system with constraints: molecular dynamics of n-alkanes. *J. Comput. Phys.* 23:327–41
88. Sanz-Serna JM, Calvo MP. 1994. *Numerical Hamiltonian Problems.* London: Chapman & Hall
89. Schlick T. 1996. Pursuing Laplace's vision on modern computers. In *Mathematical Applications to Biomolecular Structure and Dynamics*, ed. JP Mesirov, K Schulten, DW Sumners. *IMA Vol. Math. Appl.* 82:219–47. New York: Springer-Verlag
90. Schlick T. 1987. *Modeling and minimization techniques for predicting three-dimensional structures of large biological molecules.* PhD thesis. New York University, Courant Inst. Math. Sci.
91. Schlick T, Brandt A. 1996. A multigrid tutorial with applications to molecular dynamics. *IEEE Comput. Sci. Eng.* 3:78–83
92. Schlick T, Fogelson A. 1992. TNPACK—a truncated Newton minimization package for large-scale problems: I. Algorithm and usage. *ACM Trans. Math. Softw.* 14:46–70
93. Schlick T, Olson WK. 1992. Supercoiled DNA energetics and dynamics by computer simulation. *J. Mol. Biol.* 223:1089–119
94. Schlick T, Overton ML. 1987. A powerful truncated Newton method for potential energy functions. *J. Comput. Chem.* 8:1025–39
95. Schlick T, Peskin CS. 1989. Can classical equations simulate quantum-mechanical behavior? A molecular dynamics investigation of a diatomic molecule with a Morse potential. *Commun. Pure Appl. Math.* 42:1141–63
96. Schlick T, Peskin CS. 1995. Comment on: The evaluation of LI and LIN for dynamics simulations. *J. Chem. Phys.* 103:9888–89
97. Scully JL, Hermans J. 1993. Multiple time steps: limits on the speedup of molecular dynamics simulations of aqueous systems. *Mol. Simul.* 11:67–77
98. Simo JC, Tarnow N, Wang KK. 1994. Exact energy-momentum conserving algorithms and symplectic schemes for nonlinear dynamics. *Comput. Meth. Appl. Mech. Eng.* 100:63–116
99. Skeel RD, Zhang G, Schlick T. 1996. A family of symplectic integrators. *SIAM J. Sci. Comput.* 18:203–22
100. Space B, Rabitz H, Askar A. 1993. Long time scale molecular dynamics subspace integration method applied to anharmonic crystals and glasses. *J. Chem. Phys.* 99:9070–79
101. Steinbach PJ, Brooks BR. 1994. New spherical-cutoff methods for long-range forces in macromolecular simulation. *J. Comput. Chem.* 15:667–83
102. Streett WB, Tildesley DJ, Saville G. 1978. Multiple time step methods in molecular dynamics. *Mol. Phys.* 35:639–48
103. Swindoll RD, Haile JM. 1984. A multiple time-step method for molecular dynamics simulations of fluids of chain molecules. *J. Chem. Phys.* 53:289–98
104. Tobias DJ, Brooks CL III. 1988. Conformational equilibrium in the alanine dipeptide in the gas phase and aqueous solution: a comparison of theoretical results. *J. Chem. Phys.* 89:5115–26
105. Toxvaerd S. 1987. Comment on constrained molecular dynamics of macromolecules. *J. Chem. Phys.* 87:6140–43
106. Tsujishita H, Moriguchi I, Hirono S. 1993. Potential-scaled molecular dynamics and potential annealing: effective conformational search techniques for biomolecules. *J. Phys. Chem.* 97:4416–20
107. Tuckerman ME, Berne BJ. 1992. Molecular dynamics in systems with multiple time scales: systems with stiff and soft degrees of freedom and with short and long range forces. *J. Comput. Chem.* 95:8362–64
108. Tuckerman ME, Berne BJ, Martyna GJ. 1992. Reversible multiple time scale molecular dynamics. *J. Chem. Phys.* 97:1990–2001

109. Turner J, Weiner P, Robson B, Venugopal R, Schubele H III, Singh R. 1995. Reduced variable molecular dynamics. *J. Comput. Chem.* 16:1271–90
110. Turner JD, Weiner PK, Chun HM, Lupi V, Gallion S, Singh UC. 1993. Variable reduction techniques applied to molecular dynamics simulations. In *Computer Simulation of Biomolecular Systems: Theoretical and Experimental Applications,* ed. WF van Gunsteren, PK Weiner, AJ Wilkinson, Chap. 24. Leiden, The Netherlands: ESCOM
111. van Gunsteren WF. 1980. Constrained dynamics of flexible molecules. *Mol. Phys.* 40:1015–19
112. van Gunsteren WF, Karplus M. 1982. Effect of constraints on the dynamics of macro-molecules. *Macromolecules* 15:1528–43
113. Verlet L. 1967. Computer 'experiments' on classical fluids: I. Thermodynamical properties of Lennard-Jones molecules. *Phys. Rev.* 159:98–103
114. Vologodskii AV, Cozzarelli NR. 1994. Conformational and thermodynamic properties of supercoiled DNA. *Annu. Rev. Biophys. Biomolec. Struct.* 23:609–43
115. Watanabe M, Karplus M. 1993. Dynamics of molecules with internal degrees of freedom by multiple time-step methods. *J. Chem. Phys.* 99:8063–74
116. Watanabe M, Karplus M. 1995. Simulations of macromolecules by multiple time-step methods. *J. Phys. Chem.* 99:5680–97
117. Wisdom J, Holman M. 1992. Symplectic maps for the *n*-body problem: stability analysis. *Astron. J.* 104:2022–29
118. Wu J, Watts RO. 1995. Backward-Euler and other methods for simulating molecular fluids. *J. Chem. Phys.* 103:3718–32
119. Zhang G, Schlick T. 1993. LIN: a new algorithm combining implicit integration and normal mode techniques for molecular dynamics. *J. Comput. Chem.* 14:1212–33
120. Zhang G, Schlick T. 1994. The Langevin/implicit-Euler/Normal-Mode scheme (LIN) for molecular dynamics at large time steps. *J. Chem. Phys.* 101:4995–5012
121. Zhang G, Schlick T. 1995. Implicit discretization schemes for Langevin dynamics. *Mol. Phys.* 84:1077–98
122. Zhou R, Berne BJ. 1995. A new molecular dynamics method combining the reference system propagator algorithm with a fast multipole method for simulating proteins and other complex systems. *J. Chem. Phys.* 103:9444–59